January 1993 • NREL/TP-451-4851

New III-V Cell Design Approaches for Very High Efficiency

Annual Subcontract Report
1 August 1990 - 31 July 1991

M. S. Lundstrom
M. R. Melloch
G. B. Lush
G. J. O'Bradovich
M. P. Young
Purdue University
West Lafayette, Indiana

National Renewable Energy Laboratory
A Division of Midwest Research Institute
Operated for the U.S. Department of Energy
Under Contract No. DE-AC02-83CH10093

NREL/TP-451-4851 • UC Category: 272 • DE92010558

New III-V Cell Design Approaches for Very High Efficiency

Annual Subcontract Report 1 August 1990 - 31 July 1991

NREL/TP--451-4851

DE92 010558

M. S. Lundstrom
M. R. Melloch
G. B. Lush
G. J. O'Bradovich
M. P. Young
Purdue University
West Lafayette, Indiana

NREL technical monitor: J. Benner

National Renewable Energy Laboratory
(formerly the Solar Energy Research Institute)
1617 Cole Boulevard
Golden, Colorado 80401-3393
A Division of Midwest Research Institute
Operated for the U.S. Department of Energy
under Contract No. DE-AC02-83CH10093

Prepared under Subcontract No. XM-0-19142-1

January 1993

MASTER

This publication was reproduced from the best available camera-ready copy
submitted by the subcontractor and received no editorial review at NREL.

NOTICE

This report was prepared as an account of work sponsored by an agency of the United States government. Neither the United States government nor any agency thereof, nor any of their employees, makes any warranty, express or implied, or assumes any legal liability or responsibility for the accuracy, completeness, or usefulness of any information, apparatus, product, or process disclosed, or represents that its use would not infringe privately owned rights. Reference herein to any specific commercial product, process, or service by trade name, trademark, manufacturer, or otherwise does not necessarily constitute or imply its endorsement, recommendation, or favoring by the United States government or any agency thereof. The views and opinions of authors expressed herein do not necessarily state or reflect those of the United States government or any agency thereof.

Printed in the United States of America
Available from:
National Technical Information Service
U.S. Department of Commerce
5285 Port Royal Road
Springfield, VA 22161

Price: Microfiche A01
Printed Copy A04

Codes are used for pricing all publications. The code is determined by the number of pages in the publication. Information pertaining to the pricing codes can be found in the current issue of the following publications which are generally available in most libraries: *Energy Research Abstracts (ERA)*; *Government Reports Announcements* and Index (*GRA* and I); *Scientific and Technical Abstract Reports (STAR)*; and publication NTIS-PR-360 available from NTIS at the above address.

PREFACE

To realize cost-effective solar cells with efficiencies exceeding 35% is an important objective of the national photovoltaics program. Cell efficiencies are progressing rapidly, but it seems unlikely that the present design approach will produce efficiencies very much above 30% under concentration. Multi-junction cells, both monolithic and mechanically-stacked, have already achieved efficiencies well above 30%, but substantial cost reductions are still required. The objective of our research is to examine new *design* approaches for achieving very high conversion efficiencies.

The research program is divided into two thrusts with the first centering on exploring new thin-film approaches specifically designed for III-V semiconductors. By employing light trapping techniques to confine the incident photons as well as the photons emitted by radiative recombination, substantial efficiency gains may be possible. The thin-film approach is a promising route for achieving substantial performance improvements in the already high-efficiency, single-junction, GaAs cell. The potential for sizable efficiency gains along with the cell cost advantages make the thin-film approach a promising one that should be broadly applicable to III-V single- and multiple-junction cells.

The second research thrust centers on exploring design approaches for achieving high conversion efficiencies without requiring extremely high-quality material. Success in this phase of the research would benefit multiple-junction cells for which the selection of a component cell often involves a compromise between optimum bandgap and optimum material quality. It could also be a benefit in a manufacturing environment by making the cell's efficiency less dependent on material quality.

This report describes progress during the first year of this three-year project. A key part of this year's work was a collaborative effort, described in Chapter 1, involving Hugh MacMillan of Varian Associates and Richard Ahrenkiel of SERI. Without their efforts, this work could not have been accomplished.

SUMMARY

Project Overview

Our group's past work on basic studies of GaAs solar cells helped us to understand the losses that dominate in present-day cells, and it serves as the foundation for the device design research now underway. The unconventional design approaches we are exploring also require new basic research on radiative recombination, photon recycling, and AlGaAs loss mechanisms. The research program is, therefore, balanced to increase our basic understanding of III-V cell device physics and to explore the potential of unconventional cell designs.

To enhance the already high efficiency of GaAs cells, we are exploring new, thin-film approaches designed to trap incident light and to take advantage of so-called photon recycling effects. It has long been realized that radiative recombination is not necessarily a loss mechanism; *if* the cell is thick enough and *if* the emitted photons are confined within the cell. By adopting a thin-film cell approach, designed to optically confine the photons emitted by radiative recombination within the cell, lifetimes could be enhanced by an order of magnitude — or even more. Thin-film cells might also benefit from conventional, incident light trapping, which is used with great success for silicon cells.

The second research thrust centers on developing cell designs to maximize conversion efficiencies without requiring extremely high material quality. By using MBE film growth, we plan to investigate a variety of cell design options. A sound understanding of recombination losses in AlGaAs cells is a prerequisite for selecting an appropriate design, so basic work to quantify losses in AlGaAs cells is an important part of the research program.

Scientific and Technical Activities: 1990 - 1991

During the project's first year, our plans were to focus on demonstrating long lifetimes in MBE-grown GaAs, but an unexpected opportunity to work with Hugh MacMillan at Varian to characterize lifetime versus doping in high-quality MOCVD n-GaAs arose and became our main focus. Thirty-five double heterostructure (DH) films with various active layer thicknesses and seven different doping densities were grown and examined by photoluminescence (PL) decay measurements in Dick Ahrenkiel's laboratory at SERI. The results have provided a wealth of much needed but previously unavailable data for solar cell design (see Chapter 1 and publications 1-4 listed in Appendix 1). We found that even for n-GaAs doped above 10^{18} cm^{-3}, radiative recombination dominates. Strong evidence for photon recycling was observed, and the radiative lifetimes were found to be somewhat longer than for correspondingly doped p-type GaAs. These films

will also provide the samples for much of the basic studies on photon recycling planned for years 2 and 3. Although this opportunity to collaborate with researchers at Varian and SERI was not a part of the original plan, it should greatly benefit the project.

During the past year, we also had an opportunity to examine the PL decay of three MBE films doped at 10^{17} cm^{-3} and three doped at 10^{18} cm^{-3}. The PL lifetimes were found to be quite long, though not as long as those grown by MOCVD at Varian. In comparison to the MOCVD films, the MBE films show stronger evidence of Shockley-Read-Hall (SRH) recombination. At a given film thickness, we find the MBE lifetimes to be roughly 75% of those for Varian's MOCVD films. For the more lightly doped films, the SRH recombination appears to be due to bulk traps and for the more heavily doped films, to interface traps. Nevertheless, the analysis of the decay constants for the MBE samples suggest the presence of photon recycling, and the decay constants were longer than the radiative limit (assuming $B = 2 \times 10^{-10}$ cm^3/s) which suggests the presence of radiative recombination. It appears that although the lifetimes in the MBE films are not quite as long as those in very high quality MOCVD material, they are sufficient for our studies at this point. We also now have an abundance of MOCVD films suitable for the photon recycling basic studies. As the work progresses, however, we shall have to continually work to suppress SRH recombination in the MBE films.

Another objective for the project's first year was to demonstrate state-of-the-art efficiencies for $Al_{0.2}Ga_{0.8}As$ and $Al_{0.4}Ga_{0.6}As$ solar cells. In the past, we have concentrated on fabricating test structures in our laboratory and have collaborated with outside laboratories when high-efficiency cells were to be fabricated. Given the emphasis on exploring new cell designs, however, we felt that it was important to have an in-house capability for fabricating high-efficiency cells, so we devoted more effort than initially planned to this effort. For cell metalization, we turned on a new electron beam evaporation system, and for anti-reflection coatings, a new evaporator was designed, constructed, and initial evaporations have now been demonstrated. $Al_{0.2}Ga_{0.8}As$ and $Al_{0.4}Ga_{0.6}As$ films have been grown in our MBE lab. Finally, considerable work on defining and implementing a complete, high-efficiency cell fabrication process was undertaken. We plan to have a high-efficiency fabrication process implemented during the project's second year and expect that this capability will prove to be important to the project's over-all success.

Overview of the Report

This report consists of three chapters which describe last year's research activities. Chapter 1 is a detailed description of an experimental study of minority carrier recombination in n-type, MOCVD GaAs. The results have some important implications for GaAs cell design. An assessment of the minority carrier lifetimes in n-GaAs grown by MBE is the subject of Chapter 2. Although the lifetimes are not as high as those we found for MOCVD material, they should be adequate for the immediate studies we plan. Finally, Chapter 3 describes our work in developing a high-efficiency cell fabrication process.

TABLE OF CONTENTS

CHAPTER 1: MINORITY CARRIER LIFETIME in n-GaAs Grown by MOCVD 1

CHAPTER 2: ASSESSMENT of LIFETIMES in MBE-GROWN n-GaAs 21

CHAPTER 3: BASELINE AlGaAs CELL FABRICATION PROCESS 32

APPENDIX 1: AlGaAs SOLAR CELL RUN SHEET 44

APPENDIX 2: BIBLIOGRAPHY OF SERI-SUPPORTED PUBLICATIONS 47

CHAPTER 1

MINORITY CARRIER LIFETIMES

IN N-TYPE GaAs GROWN BY MOCVD

Preface

(A version of this chapter was submitted as an article to the Journal of Applied Physics.) Time-resolved photoluminescence measurements are used to explore minority carrier recombination in GaAs grown by metalorganic chemical vapor deposition, and doped n-type with selenium from 1.3×10^{17} cm^{-3} to 3.8×10^{18} cm^{-3}. For doping densities $N_D < 10^{18}$ cm^{-3}, the lifetime is found to be controlled by radiative recombination and photon recycling with no evidence of Shockley-Read-Hall recombination. For higher doping densities, samples show evidence of Shockley-Read-Hall recombination as reflected in the intensity dependence of the photoluminescence decay. Still, we find that radiative recombination and photon recycling are important for all doping concentrations studied. By separating non-radiative and radiative components to the recombination, estimates of the radiative lifetimes are given. These estimates suggest that the B coefficient decreases with increasing doping concentration.

1.1 Introduction

An understanding of how the minority carrier lifetime varies with doping is essential for designing bipolar devices such as solar cells, transistors, and lasers. In particular, it is important to understand how the radiative, Shockley-Read-Hall (SRH) and Auger lifetimes vary with doping. For p-GaAs grown by liquid phase epitaxy (LPE), extensive data are available and show that for $10^{15} \leq N_A \leq 10^{19}$ cm^{-3}, the minority electron lifetime is controlled by radiative recombination [1]. Hwang reported measurements of the minority hole lifetime in Te-doped, melt-grown n-GaAs and found that the lifetime was controlled by non-radiative, SRH processes for most doping concentrations [2-4]. A recent study by Puhlmann, *et al.* has found that Sn-doped n-GaAs grown by LPE is similarly dominated by non-radiative recombination [5]. However, the radiative and Auger lifetimes are intrinsic processes which are still not satisfactorily quantified in n-type GaAs. Garbuzov deduced radiative lifetimes in LPE-grown n-type GaAs, but his results differ from Hwang's by an order of magnitude. Few attempts at measuring the Auger coefficients have been made [5-7]. Theoretical predictions for the importance of Auger recombination in GaAs are widely varied [8-10] largely because so little supportive data is available. Neither Hwang nor Garbuzov found evidence of Auger recombination in n-type GaAs, while Puhlmann, *et al.* found an unexpectedly high Auger coefficient. Modern epitaxial growth techniques produce higher quality material which ought to yield more accurate results for the intrinsic recombination mechanisms, radiative and Auger.

In this paper we report a comprehensive study of the doping-dependent minority carrier recombination in AlGaAs/GaAs double heterostructures (DHs) grown by metalorganic

chemical vapor deposition (MOCVD) and doped n-type with selenium from 1.3×10^{17} cm^{-3} to 3.8×10^{18} cm^{-3}. Unlike Hwang and Puhlmann, *et al.*, we find that radiative recombination is the dominant mechanism for $N_D < 10^{18}$ cm^{-3} and is important at all doping concentrations. Intensity-dependent measurements show evidence for SRH recombination in films doped $N_D > 10^{18}$ cm^{-3}, and the data indicate that the radiative coefficient may decrease with increasing doping in n-GaAs.

The paper is organized as follows. An outline of the analysis procedure for the DHs is given in Sec. 2. The MOCVD growth techniques are described in Sec. 3 where the DHs grown for the study are listed. The experimental apparatus and techniques for measuring the time-resolved photoluminescence decay are also described in Sec. 3. In Sec. 4 we present the results for both low- and high-intensity laser excitation. The measured results are analyzed in Sec. 4, and deduced lifetimes of the several mechanisms are given. In Sec. 5 we show by further analysis that the data indicate that radiative recombination and photon recycling are important at all doping concentrations. Finally, we summarize the results and conclusions in Sec. 6.

1.2 Procedure for Double Heterostructure (DH) Analysis

Observing the photoluminescence decay of DHs has become a popular technique for the determination of interface and bulk recombination parameters [11, 12]. Under easily achievable conditions which produce a flat carrier distribution in the DH, one can express the decay constant of a DH as [13],

$$\frac{1}{\tau_{DH}} = \frac{1}{\tau_{bulk}} + \frac{2S}{d}, \tag{1.1a}$$

where the bulk lifetime is defined as

$$\frac{1}{\tau_{bulk}} = \frac{1}{\tau_r} + \frac{1}{\tau_{SRH}} + \frac{1}{\tau_{Auger}}. \tag{1.1b}$$

Here, S is the average of the front and back interface recombination velocities, d is the DH thickness, and τ_{bulk} is made up of contributions from the radiative, SRH, and Auger mechanisms, respectively. Equations (1) clearly show contributions to τ_{DH} from both the interfaces and from the several bulk mechanisms. In this section we outline the steps taken and issues confronted in determining the minority carrier lifetimes and recombination velocities of these mechanisms by observing photoluminescence decay. We find that we are able to set upper limits on S, lower limits on the non-radiative lifetime and then compute the bounds on the radiative lifetimes for each doping concentration.

In order to quantify experimentally the contributions from each of the recombination mechanisms, the τ_{DH} of several DHs of varying thickness at a specific doping concentration

must be measured. To separate the bulk contribution from that of the interfaces, a plot of $1/\tau_{DH}$ versus $2/d$ is constructed. According to Eq. (1a), the intercept of this line is $1/\tau_{bulk}$, and the slope of this line is taken to be the average of S_f and S_b, the front and back interface recombination velocities, respectively. However, in all cases reported here, we found that these plots were decidedly non-linear, making determination of a unique S impossible. It is only possible then to place an upper limit on S based on the decay constants of the two thinnest DHs. One could explain this non-linearity by a thickness dependence of the effective interface recombination velocities, S_{eff}. However, we discuss data and analysis in Secs. 4 and 5 that show that this curvature can better be explained by photon recycling.

Photon recycling is the reabsorption of photons emitted during a radiative recombination event, which creates a new electron-hole pair. Photon recycling increases the observed minority carrier lifetime of GaAs when radiative recombination is important. The bulk lifetime is then rewritten as

$$\frac{1}{\tau_{bulk}} = \frac{1}{\phi_r \tau_r} + \frac{1}{\tau_{SRH}} + \frac{1}{\tau_{Auger}}, \tag{1.2}$$

where ϕ_r, Asbeck's recycling cofactor [14], is the inverse of the probability that an isotropically emitted photon escapes the active volume of a DH with a flat distribution of excited carriers. Since photons are only lost at the interfaces, an average photon emitted isotropically is more likely to be reabsorbed in a thicker DH. This results in a thickness dependence on the bulk lifetime, as a thicker DH will seem to have a longer radiative lifetime [14-16]. Since τ_{bulk} increases with DH thickness, the value of S that we deduce will be an upper limit.

In light of these observations, the first step in the analysis of a series of DHs is to set the upper limit of S (which we found to contribute little to recombination for $N_D \geq 10^{18}$ cm^{-3}). The second step in the analysis is to separate radiative recombination from non-radiative bulk recombination by accounting for photon recycling. Neglecting $2S/d$ for large d, we can write the DH decay constant as

$$\tau_{DH} = \frac{\phi_r \tau_r \tau_{nr}}{\phi_r \tau_r + \tau_{nr}} \tag{1.3}$$

where τ_{nr} is a combination of the SRH and Auger lifetimes. Since $\phi_r \tau_r$ becomes large as d becomes large, τ_{DH} should approach the non-radiative bulk lifetime for the thickest DHs even if the assumption of a flat carrier distribution is not valid for the thicker and more heavily doped DHs. The decay constant of the thickest DH at each doping concentration is thus a lower limit for the non-radiative lifetime at that doping level.

The final step is to subtract the contributions of these non-radiative surface and bulk mechanisms from the total recombination of the thinnest DH. This difference yields the $\phi_r \tau_r$

n-$Al_{0.3}Ga_{0.7}As$	$2x10^{18}$ cm^{-3}	500 Å
n-GaAs Active Layer		
n-$Al_{0.3}Ga_{0.7}As$	$2x10^{18}$ cm^{-3}	1500 Å
n-$Al_{0.85}Ga_{0.15}As$	$2x10^{18}$ cm^{-3}	500 Å
p^+ GaAs Buffer Layer		
p^+ GaAs Substrate		

Figure 1.1 Basic structure of the double heterostructures (DHs) grown by metalorganic chemical vapor deposition. Laser illumination and luminescence detection occur at the top.

product for that DH at a specific doping concentration. Values for ϕ_r from the literature [16] allow determination of τ_r. Thus from a series of DHs of differing thicknesses at a specific doping concentration, one can estimate the parameters determining the rates for the radiative and the surface and bulk non-radiative recombination mechanisms. The relative importance of each of these bulk mechanisms changes with doping, and it is the crux of this paper to quantify the parameters for each mechanism.

1.3 Film Growth Methods

The DHs were grown at 740°C under atmospheric pressure by MOCVD in a horizontal reactor at the Varian Research Center. Zinc-doped, horizontal-Bridgman substrates were heated by radio frequency induction. The susceptor was molybdenum, coated with GaAs. The growth rate was six microns per hour except for the films doped to 2.4×10^{18} cm^{-3}, for which the growth rate was four microns per hour. Hydrogen selenide (from Scott Specialty Gases) diluted to 55 p.p.m. with hydrogen was the doping agent, and trimethyl aluminum, trimethyl gallium, and 100% Arsine were the sources. The V/III ratio was 30, with the exception of the films doped to 2.4×10^{18} cm^{-3}, for which the V/III ratio was 45. Hydrogen was purified by diffusion through palladium to provide a background flow rate of 12 liters/min.

Double Heterostructure Parameters					
N_D(cm^{-3})	Targeted Thicknesses(μm)				
1.3×10^{17}	0.25	1.25	2.5	5.0	10.
3.7×10^{17}	0.25	1.25	2.5	5.0	10.
1.0×10^{18}	0.5	1.0	2.0	4.0	8.
2.2×10^{18}	0.25	1.25	2.5	5.0	10.
2.4×10^{18}	0.25	0.5	1.25	2.5	10.
3.8×10^{18}	0.25	0.5	1.25	2.5	10.

Table 1.1 List of targeted thicknesses and measured doping concentrations for the double heterostructures (DHs) grown for this study. Doping concentrations were determined by van der Pauw measurements on the thickest DHs.

The basic structure of the DHs is shown in Fig. 1.1, and Table 1.1 lists the DHs grown for this study. $Al_{0.3}Ga_{0.7}As$ layers provide passivation and carrier confinement. The back two AlGaAs layers serve these purposes and serve as etch stop or etch release layers as well [17, 18]. All doping concentrations were measured by the van der Pauw technique.

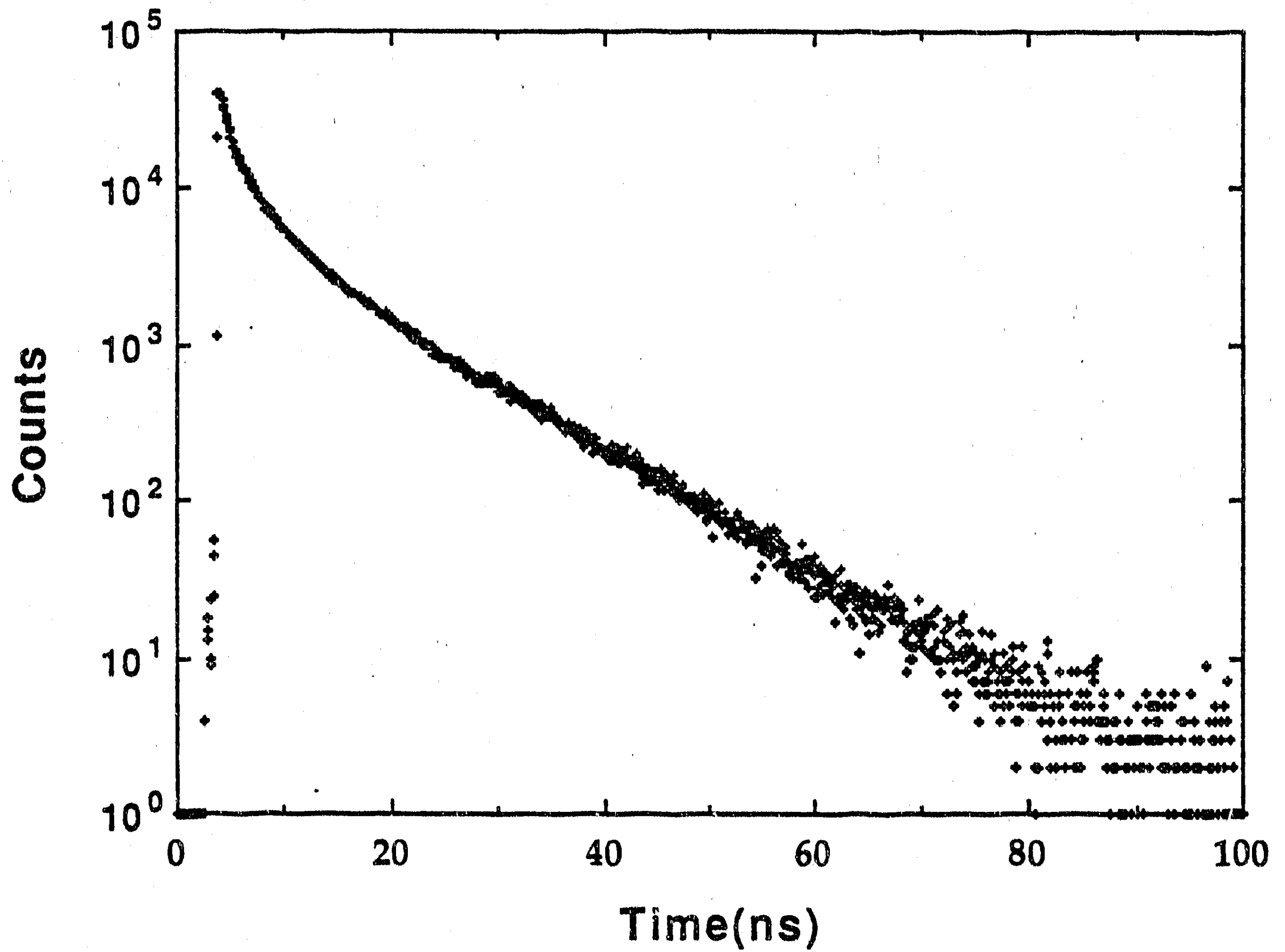

Figure 1.2 Typical decay of photoluminescence intensity as observed from a AlGaAs/GaAs double heterostructure (DH). This DH is 1.0 μm thick, doped to 10^{18} cm^{-3}, and is under 20 milliwatts intensity over a one centimeter illumination spot size.

Photoluminescence decay was observed by the time-correlated, single photon counting technique described previously [19]. The DHs are illuminated with light of wavelength 600 nanometers at intensities from 0.1 to 20 milliwatts with a one centimeter diameter spot size. A typical decay is shown in Fig. 1.2. This DH has a 1.0 μm thick active area doped 10^{18} cm^{-3} and is under 20 milliwatts illumination. The initial fast decay is due to radiative recombination under high injection. A least squares fit to the natural log of the data yields the DH decay constant.

1.4 Results

Table 1.2 lists the decay constants and uncertainty under low intensity excitation for each DH studied. Figure 1.3 plots these data points versus doping along with the theoretical radiative limit defined as

$$\tau_r = \frac{1}{BN_D}, \tag{1.4}$$

using a B coefficient of 2.0×10^{-10} cm^3/sec [20]. Note that the lifetimes of all DHs, including non-radiative mechanisms, are longer than this theoretical estimate.

Figure 1.4 shows plots of $1/\tau_{DH}$ versus $2/d$ for several doping concentrations. As mentioned earlier, all are non-linear. Non-linearity in these plots can come about by either a change in S_{eff} with DH thickness or by photon recycling, but we show in Sec. 5 that the most likely explanation is photon recycling. Table 1.3 lists the upper limits of S for each DH series. Using Eqs. (1) and assuming τ_{bulk} is constant, the upper limit of S was computed by

$$S = \frac{1}{2}\frac{1/\tau_{DH1} - 1/\tau_{DH2}}{1/d_1 - 1/d_2}, \tag{1.5}$$

where the subscripts one and two refer to the thinnest DH and the second most thin DH, respectively, at each doping concentration. We find that interface recombination strongly contributes to the decay constant only for the thinnest DHs with $N_D \leq 3.7 \times 10^{17}$ cm^{-3}. Later we will show that the bulk recombination of all DHs with $N_D < 10^{18}$ cm^{-3} is dominated by radiative recombination. Knowing this, a more accurate estimate for S is obtained by accounting for the change in τ_{bulk} due to photon recycling. If $\tau_{bulk} = \phi_r \tau_r$, Eq. (5) is rewritten as

$$S = \frac{1}{2}\frac{\phi_{r1}/\tau_{DH1} - \phi_{r2}/\tau_{DH2}}{\phi_{r1}/d_1 - \phi_{r2}/d_2} \tag{1.6}$$

Using values for ϕ_r taken from Miller [16], we find more reasonable values of S to be 33 cm/s

Double Heterostructure (DH) Decay Times					
N_D (cm^{-3})	DH Decay Constant (ns)				
1.3×10^{17}	65 ± 5	145 ± 5	210 ± 5	330 ± 10	465 ± 5
3.7×10^{17}	21 ± 2	48 ± 2	65 ± 3	106 ± 2	154 ± 4
1.0×10^{18}	9 ± 2	10 ± 1	12 ± 0.5	17.5 ± 1	24 ± 2
2.2×10^{18}	4 ± 0.5	4.8 ± 0.5	5.5 ± 0.5	7.2 ± 0.2	8.8 ± 0.2
2.4×10^{18}	2.48 ± 0.1	2.52 ± 0.1	2.75 ± 0.5	3.1 ± 0.1	3.2 ± 0.1
3.8×10^{18}	1.7 ± 0.2	1.75 ± 0.25	1.9 ± 0.1	2.4 ± 0.2	3.4 ± 0.2

Table 1.2 List of the decay constant and uncertainty under low intensity excitation for each double heterostructure studied. Decay constants were determined by least squares fit to the logarithm of the data.

Upper Limits of Recombination Velocities	
N_D (cm^{-3})	S (cm/s)
1.3×10^{17}	115
3.7×10^{17}	417
1.0×10^{18}	454
2.2×10^{18}	648
2.4×10^{18}	157
3.8×10^{18}	412

Table 1.3 List of the upper limit of the interface recombination velocity for each series as computed from Eq. 4. More reasonable values for $N_D = 1.3 \times 10^{17}$ cm^{-3} and $N_D = 3.7 \times 10^{17}$ cm^{-3} found by incorporating recycling theory are 33 cm/s and 124 cm/s, respectively.

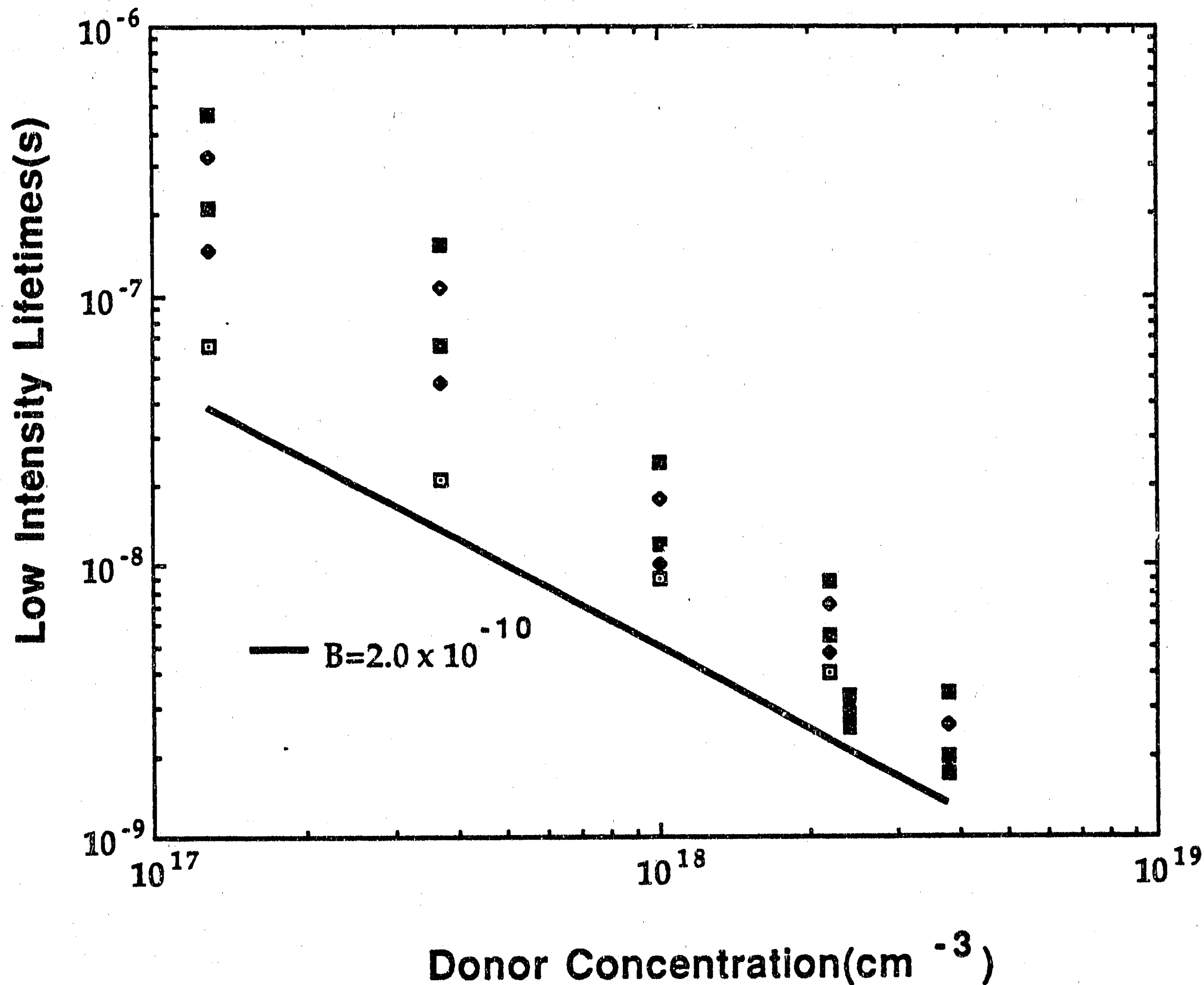

Figure 1.3 Plot of decay constants for every double heterostructure under low intensity excitation. Note that every τ_{DH} is greater than the theoretical radiative limit found by using $B = 2.0 \times 10^{-10}$ cm^3/s in Eq. (4).

and 124 cm/s for the 1.3×10^{17} cm^{-3} and 3.7×10^{17} cm^{-3} DHs respectively.

After determining S, the next step is to determine the radiative and non-radiative contributions to the bulk recombination. These can be found by looking at a plot of τ_{bulk} versus DH thickness. Figure 1.5 shows τ_{bulk} versus DH thickness for $N_D < 10^{18}$ cm^{-3}. τ_{bulk} is found by subtracting the interface contribution to recombination from τ_{DH}, using the more reasonable values for S. The solid line in Fig. 1.5 represents the expected dependence of the bulk lifetime if the change in τ_{bulk} were due solely to radiative recombination and photon recycling. The data closely follow recycling theory. We believe this is indicative of material dominated by radiative recombination with the observed lifetime enhanced by photon recycling.

By assuming that photon recycling is responsible for the changes in lifetime with DH thickness, we can now use Eq. (3) to deduce a lower limit for the non-radiative lifetime for DHs with $N_D > 10^{18}$ cm^{-3}. Figure 1.6 shows τ_{DH} versus d for several high doping concentrations. Figure 1.6 may, at first glance, look similar to Fig. 1.5. However, the ratio of the largest and smallest DH decay constants is about two for the DH series represented in Fig. 1.6 while the ratio of the bulk lifetimes is about six for the series in Fig. 1.5. This means that τ_{DH} is saturating at a value we take to be the non-radiative bulk lifetime. Since the DHs doped $N_D \leq 10^{18}$ cm^{-3} do not show this saturation, we estimate τ_{nr} from the thickest DH to be much longer than any τ_{DH} observed. The $\phi_r\tau_r$ product is then computed by subtracting the non-radiative contributions (surface and bulk) from the decay constant of the thinnest DH. Since the non-radiative lifetime, as will be discussed below, is dependent on the injection level, it is important to compare DH decay constants measured at similar levels of injection. Therefore, the following analysis was done using low intensity data for $N_D < 10^{18}$ cm^{-3}, and high intensity data for the other doping concentrations.

Figure 1.7 displays deduced radiative lifetimes with uncertainties. (It is helpful now to refer back to Eqs. (1) and (2).) The data point represents τ_{DH} for the thinnest DH after the contribution from τ_{nr} estimated from the thickest DH is subtracted. It is not our estimate for the radiative lifetime. By subtracting the contribution to the total recombination from the interfaces (found from the upper limit of S in Table 1.1, or from the more reasonable values of S for $N_D < 10^{18}$ cm^{-3}), we obtain the upper limit of the error bars. The lower limit of the error bars is obtained by dividing the value at the data point by the value of ϕ_r obtained from the literature [16] (essentially this assumes S=0). It has been shown that ϕ_r decreases with increasing doping concentration for a given DH thickness [14]. The values of ϕ_r we use here are valid only in the range of doping concentration near $N_D = 2.0 \times 10^{17}$ cm^{-3}, so ϕ_r is increasingly overestimated for greater N_D. Therefore, in Fig. 1.7 the lower limits of the radiative lifetimes for more highly doped n-GaAs are too low. Also shown for reference is the theoretical τ_r as computed by setting $B = 2.0 \times 10^{-10}$ cm^3/s.

Two aspects immediately stand out. First, the lifetimes deduced are longer than the typically assumed value; second, the B coefficient seems to decrease for the highest doping concentrations. The apparent change in B would be more significant for higher N_D if ϕ_r were better known. Hwang also reported a decrease in B for n-type GaAs although his results differ

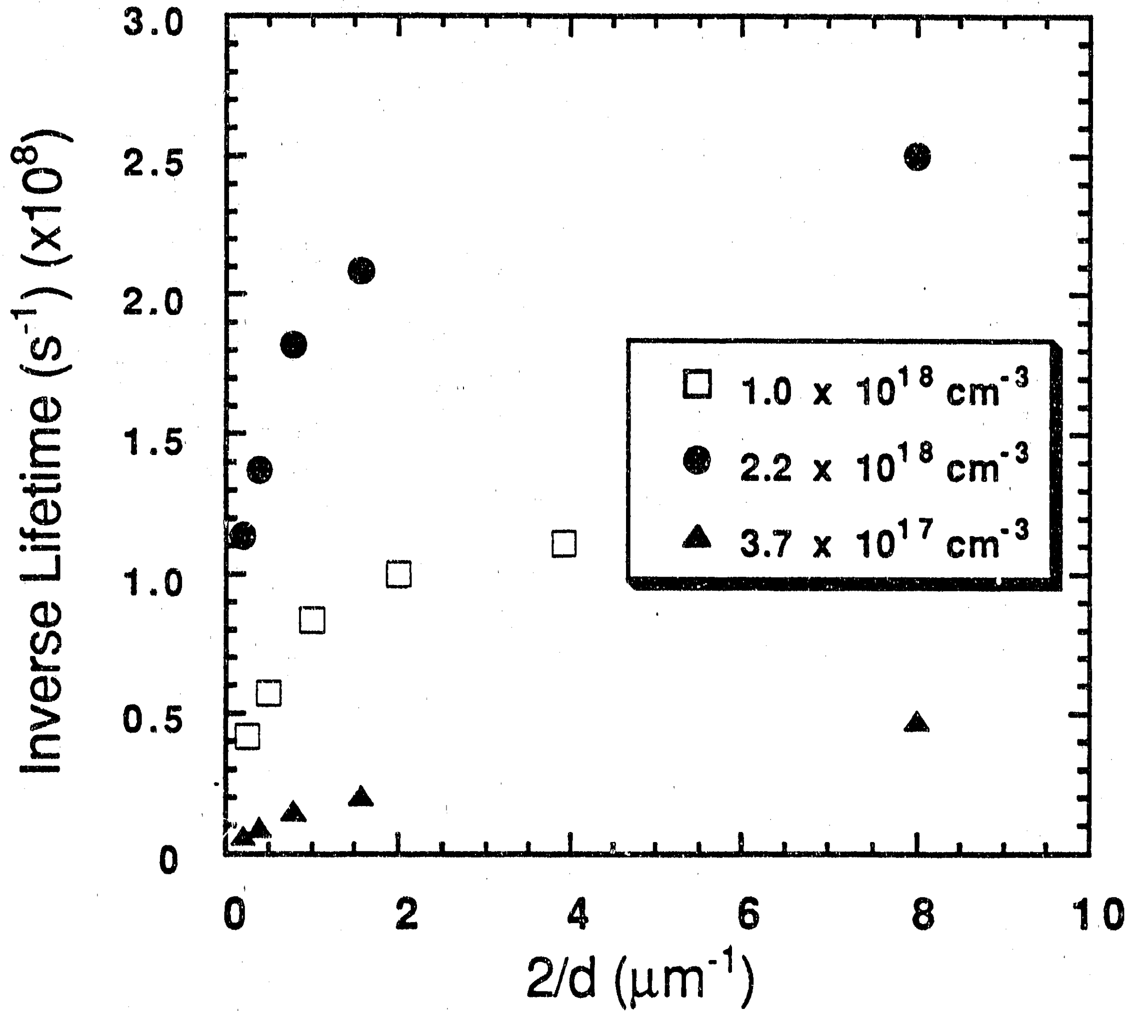

Figure 1.4 Plots of $1/\tau_{DH}$ versus 2/d for several doping concentrations. Note that all are non-linear making it impossible to determine a unique value for the interface recombination velocity from the slope of the curve. The negative curvature is evidence for photon recycling.

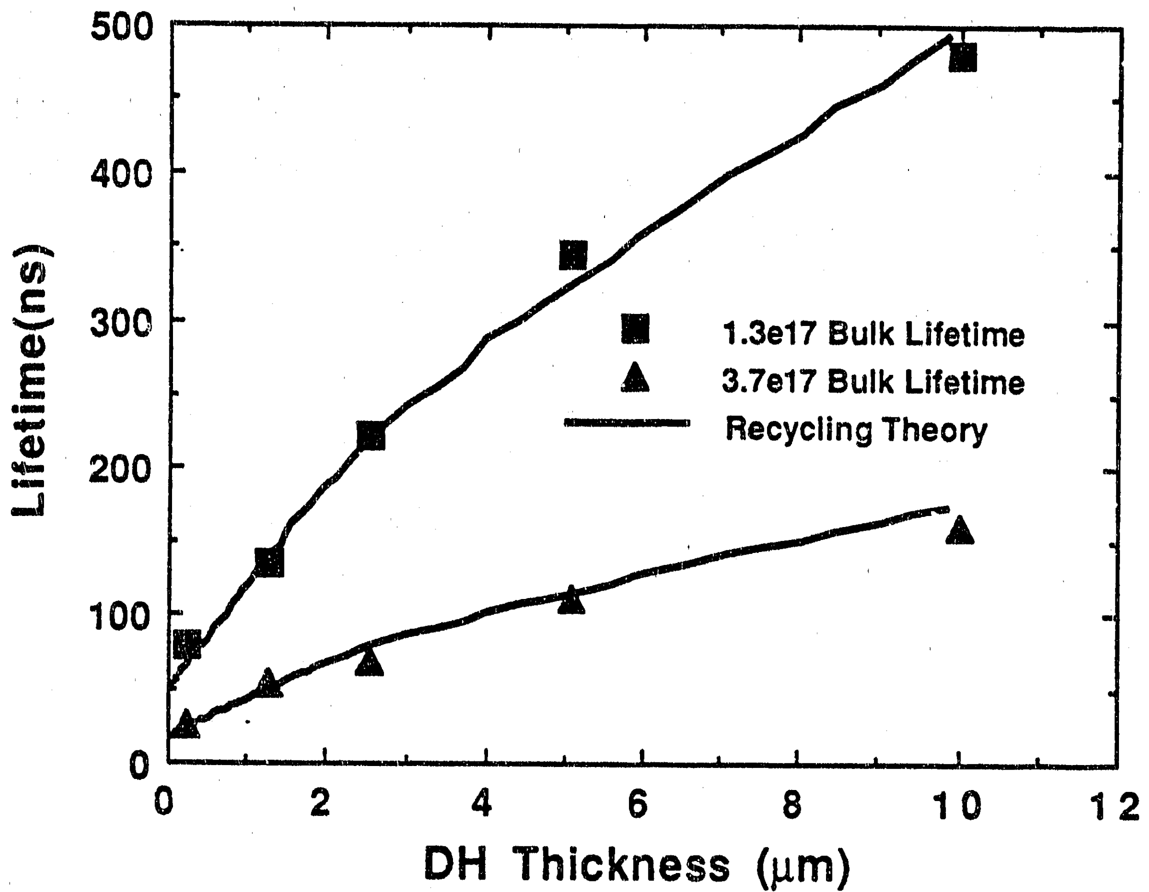

Figure 1.5 Plot of τ_{bulk} versus DH thickness for $N_D < 10^{18}$ cm^{-3}. The interface contribution is subtracted off from τ_{DH} using more reasonable values for S mentioned in the text. One can see that the bulk lifetime behaves in a manner consistent with photon recycling theory over a large range of DH thickness. The ratio of the longest and shortest bulk lifetimes is nearly six.

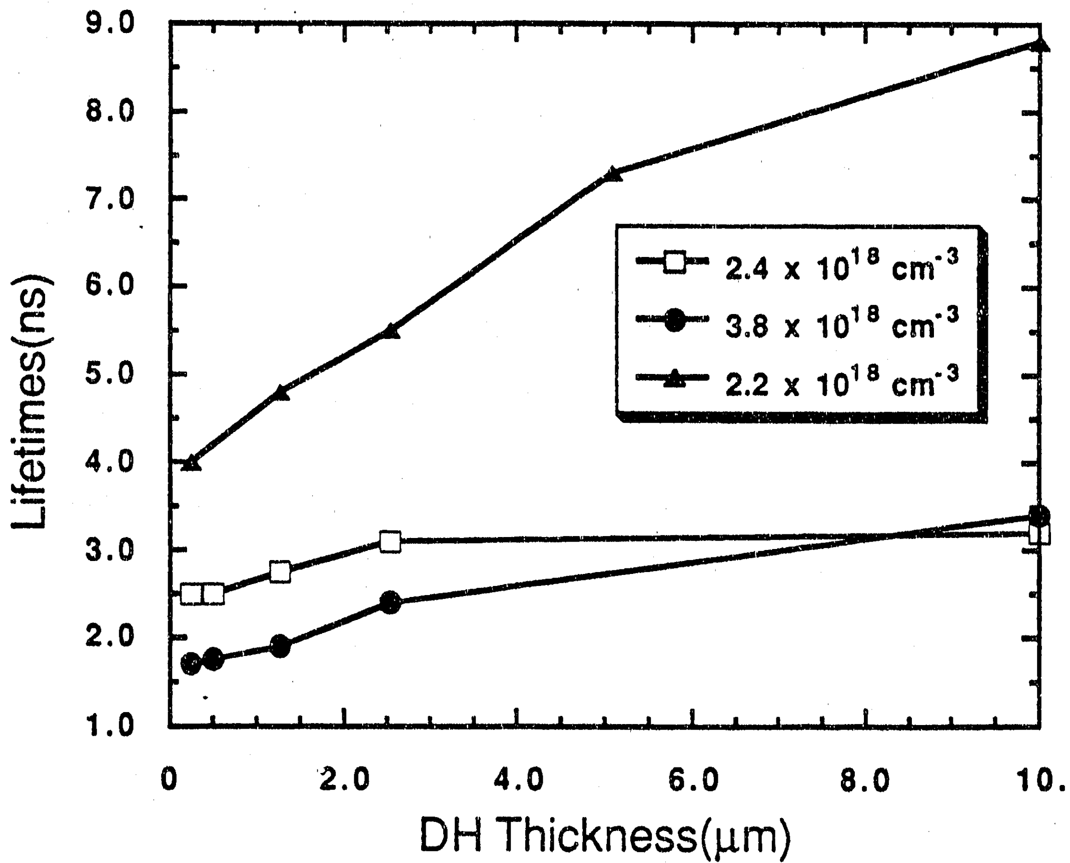

Figure 1.6 Plot of τ_{DH} versus DH thickness for several high doping concentrations. The decay constants show a tendency to saturate for thicker layers, which is expected according to Eq. (3) because $\phi_r\tau_r$ becomes large in thick DHs. The ratio of the longest and shortest bulk lifetimes is at most about two.

quantitatively from ours. This decrease in B has been attributed to the filling of electron states, commonly referred to as the Burstein shift [4,21].

Finally, it is of interest to identify the mechanism for the non-radiative bulk recombination for the DHs with $N_D > 10^{18}$ cm^{-3}. For some of these DHs, a single lifetime could not be fit to the decay for high-intensity excitation. Figure 1.8 shows this for the 10. μm thick DH doped to 3.8×10^{18} cm^{-3}. We attribute this to the saturation of SRH deep levels under high intensity, but not high injection conditions [22]. Under these conditions and if $\tau_n \gg \tau_p$, the deep levels can become emptied and the SRH recombination equation reduces to

$$R = \frac{\Delta p}{\frac{\Delta p}{N_D}\tau_n + \tau_p} \tag{1.7}$$

where Δp is the excess carrier concentration. This shows that the effective SRH lifetime is longer under high intensity than τ_{SRH} under low intensity conditions. We know that low injection conditions exist because we don't see the initial fast decay seen in Fig. 1.2. This effect is more evident at higher doping concentrations as the SRH lifetime becomes shorter and comparable to the radiative lifetime. It is also most prominent in the films doped 2.4×10^{18} cm^{-3}, which were grown at a slower growth rate than the other DHs. These films show the least variation in decay constant with DH thickness, which is indicative of material dominated by non-radiative recombination rather than radiative recombination and photon recycling. Thus, we believe that the non-radiative lifetime is dominated by SRH deep levels in the DHs doped to $N_D > 10^{18}$ cm^{-3}.

We are unable to determine the contribution from Auger recombination with the measurements reported here. None the less, we can set an upper limit on C_n if we attribute all the recombination in a DH to Auger mechanisms. We find that under high intensity excitation, the decay constant of the 10 μm thick DH doped to 3.8×10^{18} cm^{-3} yields an upper limit for C_n of 1.6×10^{-29} cm^6/s, which is an order of magnitude smaller than $C_n = 1.5 \times 10^{-28}$ cm^6/s deduced by Puhlmann, *et al.* Haug computed the Auger coefficient, C_n, theoretically to be 0.47×10^{-29} cm^6/s in n-type GaAs [9]. Since SRH recombination is significant in our DHs at higher doping concentrations, the actual value of C_n in our material must be significantly smaller so Haug's computation is not inconsistent with our results.

1.5 Discussion

Our analysis of the DHs and the results they have provided depend on our assumption that the films were dominated by radiative recombination and photon recycling. Is there another explanation? Equations (1) are not valid for the thicker DHs doped $N_D \geq 10^{18}$ cm^{-3} because the shorter lifetimes prevent establishment of a flat carrier distribution before the luminescence

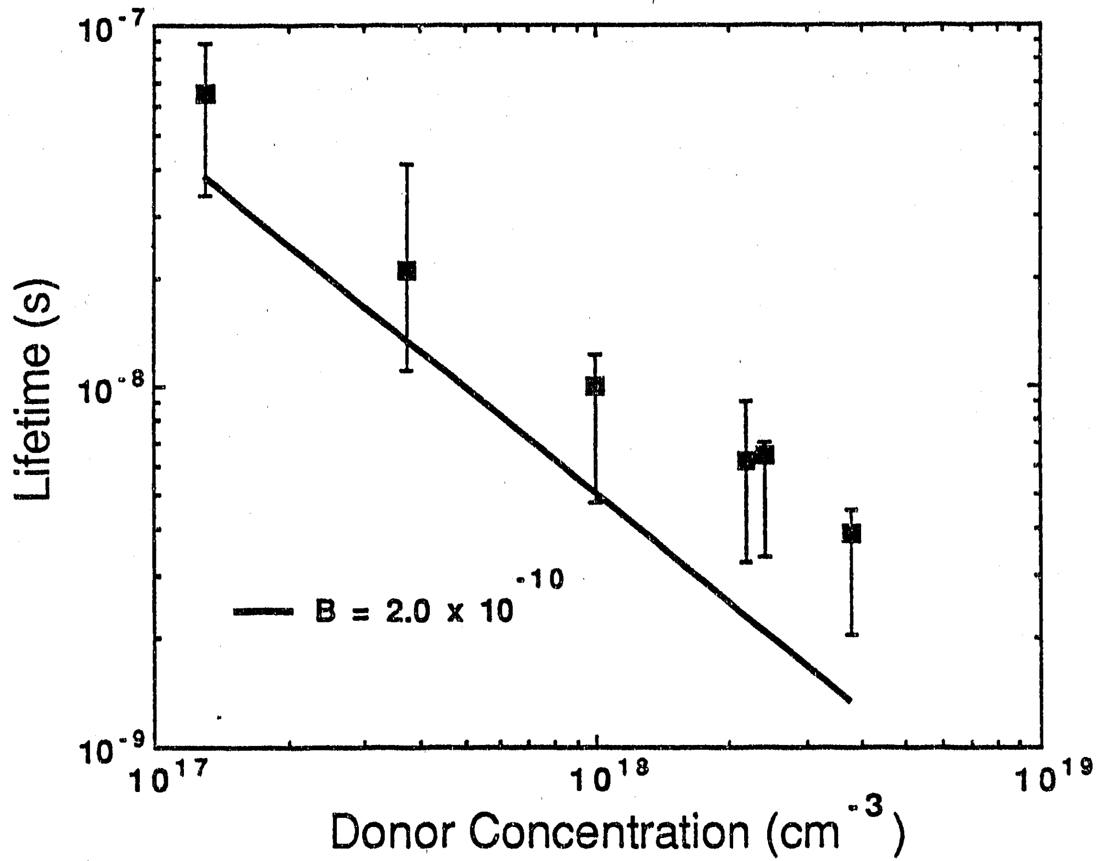

Figure 1.7 Plot of the ranges of the deduced radiative lifetimes. Also shown is the theoretical τ_r as computed by setting $B = 2.0 \times 10^{-10}$ cm^3/s. The data suggest that B may become smaller with increasing doping.

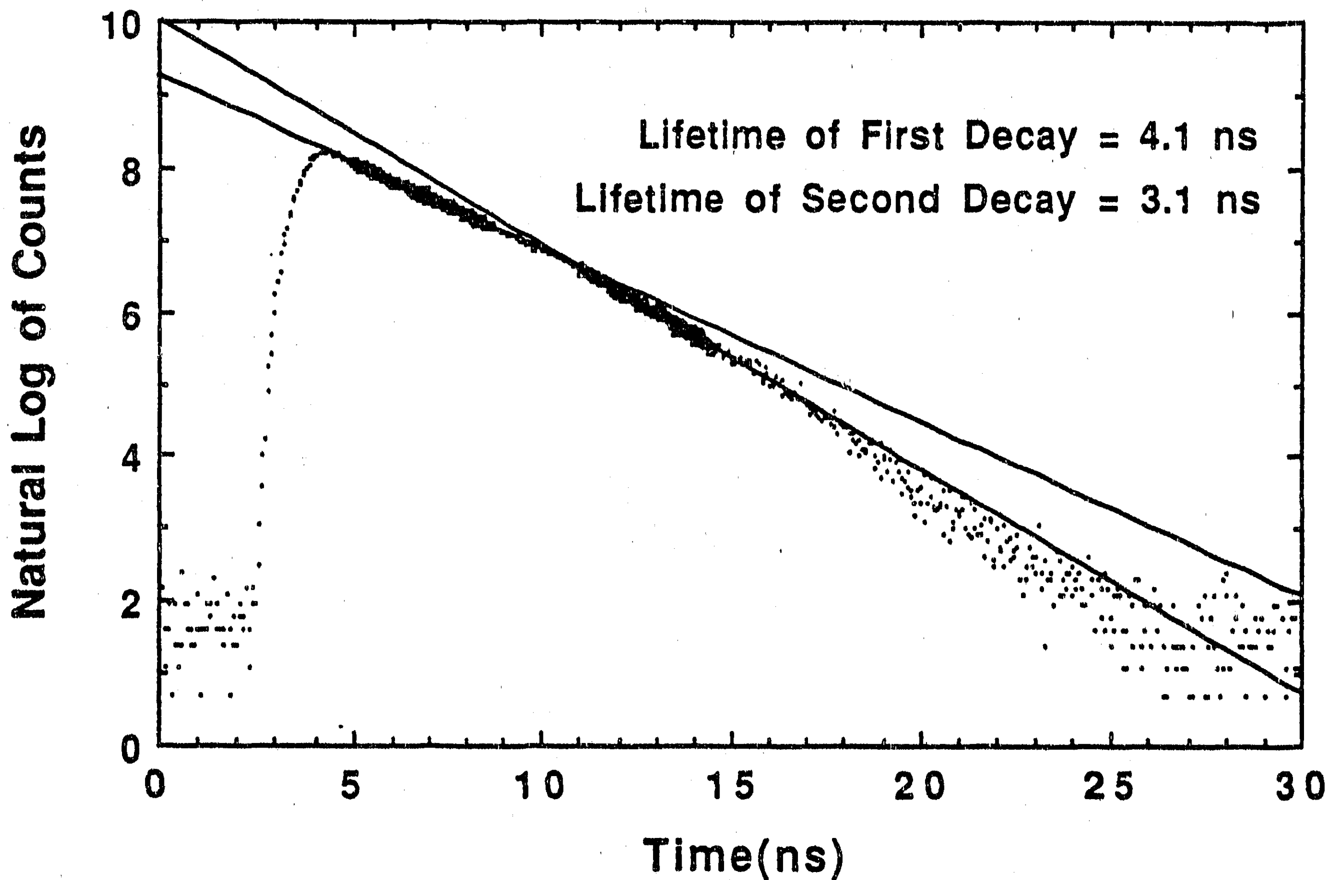

Figure 1.8 Plot of natural log of photoluminescence intensity versus time, showing two separate regions of differing decay constant. This double heterostructure is 10. μm thick, doped to 3.8×10^{18} cm^{-3}. We attribute these two rates of decay to the saturation of Shockley-Read-Hall deep levels under high intensity (but not high injection conditions) which increases the effective hole lifetime as shown in Eq. (7).

signal becomes too weak to detect. Despite this, an exponential luminescence decay is observed after some time, at which point we determine τ_{DH}. At the time when we determine τ_{DH} experimentally, fewer carriers are at the back interface so it's contribution to the total recombination is effectively diminished. It is then possible to explain a non-linear $1/\tau_{DH}$ versus 2/d plot by assuming a high S_b. Further, it has been shown in films grown by molecular beam epitaxy that the back interface can be of significantly poorer quality than the front interface [23]; such could also be the case for material grown by MOCVD.

However, referring back to Fig. 1.4, we saw that the slope of $1/\tau_{DH}$ versus 2/d is S_{eff}, the average of the front and back effective interface recombination velocities. If the change in observed lifetime were due to a decrease in S_{eff}, one would expect the slope of $1/\tau_{DH}$ versus 2/d to decrease for larger d. In other words one would expect a curve with positive curvature. Instead, $1/\tau_{DH}$ versus 2/d has negative curvature for all doping concentrations reported here.

Additionally, Eqs. (1) are valid for all our DHs if $N_D \leq 3.7 \times 10^{17}$ cm^{-3}. The $1/\tau_{DH}$ versus 2/d plots for these doping levels, like all others, display negative curvature. We also observed in Fig. 1.5 that the bulk lifetimes for $N_D < 10^{18}$ cm^{-3} behaved in a manner consistent with recycling theory. Finally, we performed computer simulations of the highly doped DHs using a finite difference solution to the minority carrier diffusion equation. Using a constant S_b and a constant bulk lifetime which was too short to establish a flat carrier distribution, the $1/\tau_{DH}$ versus 2/d plots show positive curvature. These arguments reaffirm our statement that the thickness dependence of the decay constant is largely a bulk effect and is evidence for photon recycling.

1.6 Conclusions

We have estimated the radiative lifetimes for n-type GaAs with 1.3×10^{17} cm^{-3} $< N_D <$ 3.8×10^{18} cm^{-3}. We have shown that the radiative lifetimes deduced are longer than previously believed, based upon the commonly used value for the radiative coefficient, $B = 2.0 \times 10^{-10}$ cm^3/s, but shorter than the results reported by Hwang [2-4] or by Puhlmann, *et al.* [5] We find, like Hwang, that the B coefficient seems to decrease with increasing doping. Unlike Hwang and Puhlmann, *et al.*, we find that radiative recombination dominates for $N_D \leq 10^{18}$ cm^{-3}, and is important for all doping concentrations studied.

We also have shown evidence that photon recycling is important at all doping concentrations, and has a significant effect, creating a thickness dependence of the observed lifetime. We observed evidence that the non-radiative bulk recombination for $N_D > 10^{18}$ cm^{-3} is dominated by SRH mechanisms. Finally, we found an upper limit for the Auger coefficient for n-type GaAs.

In order to better quantify the radiative lifetime, photon recycling must be better understood. Values for ϕ_r at higher doping concentrations are needed, but before that, more consistency in the data for the absorption coefficient near the band edge in n-GaAs must be found [24]. Future luminescence efficiency measurements as a function of incident intensity will

allow better assessment of the Auger recombination coefficient.

References

1. R. K. Ahrenkiel, *Minority Carrier Lifetime in Compound Semiconductors*, 3, Academic Press, New York, 1988. Current Topics in Photovoltaics, Chapter 1
2. C. J. Hwang, "Optical Properties of n-Type GaAs. I. Determination of Hole Diffusion Length from Optical Absorption and Photoluminescence Measurements," *J. Appl. Phys.*, vol. 40 (9), p. 3731, August 1969.
3. C. J. Hwang, "Doping Dependence of Hole Lifetime in n-type GaAs," *J. Appl. Phys.*, vol. 42 (11), p. 4408, October 1971.
4. C. J. Hwang, "Quantum Efficiency and Radiative Lifetime of the Band-to-Band Recombination in Heavily Doped n-type GaAs," *Phys. Rev. B*, vol. 6 (4), p. 1355, 15 August 1972.
5. N. Puhlmann, G. Oelgart, V. Gottschalch, and R. Nemitz, "Minority Carrier recombination and internal quantum yield in GaAs:Sn by means of EBIC and CL," *Semiconductor Science and Technology*, vol. 6, p. 181, 1991.
6. L. Jastrzebski, J. Lagowski, H. C. Gatos, and W. Walukiewicz, "Minority Carrier Lifetime in GaAs at Elevated Temperatures: Implications for Solar Cell Performance," *Gallium Arsenide and Related Compounds*, p. 437, Institute of Physics, London, 1979.
7. D. Z. Garbuzov, *Semiconductor Optoelectronics*, pp. 305-343, Wiley, New York, 1980. Marian A. Herman (Ed.)
8. Masumi Takeshima, "Effect of Auger Recombination on Laser Operation in $Ga_{1-x}Al_xAs$," *J. Appl. Phys.*, vol. 58 (10), p. 3846, 15 November 1985.
9. A. Haug, "Auger Recombination in Direct-gap Semiconductors: Band-Structure Effects," *J. Phys C.*, vol. 16, pp. 4159-4172, 1983.
10. L. R. Weisberg, "Auger Recombination in GaAs," *J. Appl. Phys.*, vol. 39 (13), p. 6096, December 1968.
11. R. K. Ahrenkiel, D. J. Dunlavy, Brian Keyes, S. M. Vernon, T. M. Dixon, S. P. Tobin, K. L. Miller, and R. E. Hayes, "Ultralong Minority-carrier Lifetime in Epitaxial GaAs by Photon Recycling," *Appl. Phys. Letters*, vol. 55(11), p. 1088, 11 September 1989.
12. J. M. Olson, R. K. Ahrenkiel, D. J. Dunlavy, Brian Keyes, and A. E. Kibbler, "Ultralow Recombination Velocity at $Ga_{0.5}In_{0.5}P$/GaAs Heterointerfaces," *Appl. Phys. Lett.*, vol. 55 (12), p. 1208, 18 September 1989.
13. A. Many, Y. Goldstein, and N. B. Grover, *Semiconductor Surfaces*, John Wiley and Sons, New York, 1965.
14. P. Asbeck, "Self-absorption Effects on the Radiative Lifetime in GaAs-GaAlAs Double Heterostructures," *J. Appl. Phys.*, vol. 48 (2), p. 820, February 1977.
15. R. J. Nelson and R. G. Sobers, "Minority-carrier Lifetime and Internal Quantum Efficiency of Surface-free GaAs," *J. Appl. Phys.*, vol. 49 (12), p. 6103, December 1978.
16. K. L. Miller, *Analysis of Transient Photoluminescence From $Al_xGa_{1-x}As$/GaAs Double Heterostructure Samples*, University of Colorado, at Boulder, 1989. M.S.E.E. Thesis
17. Eli Yablanovitch, T. Gmitter, J. P. Harbison, and R. Bhat, "Extreme Selectivity in the Lift-off of Epitaxial GaAs Films," *Appl. Phys. Lett.*, vol. 51 (26), p. 2222, 28 December 1987.
18. D. D. Sell and H. C. Casey, Jr., "Optical Absorption and Photoluminescence Studies of thin GaAs Layers in GaAs--$Al_xGa_{1-x}As$ Double Heterostructures," *J. Appl. Phys.*, vol. 45 (2), p. 800, February 1974.
19. R. K. Ahrenkiel, D. J. Dunlavy, and T. Hanak, "Minority-carrier lifetime in ITO/InP heterojunctions," *J. Appl. Phys.*, vol. 64 (4), p. 1916, 15 August 1988.

(2), p. 800, February 1974.

19. R. K. Ahrenkiel, D. J. Dunlavy, and T. Hanak, "Minority-carrier lifetime in ITO/InP heterojunctions," *J. Appl. Phys.*, vol. 64 (4), p. 1916, 15 August 1988.
20. H. C. Casey, Jr. and M. B. Panish, *Heterostructure Lasers*, Academic Press, New York, 1978.
21. E. Burstein, "Anomalous Optical Absorption Limit in InSb," *Phys. Rev.*, vol. 93, p. 632, 1954.
22. R. K. Ahrenkiel, B. M. Keyes, and D. J. Dunlavy, "Intensity-Dependent Minority-Carrier Lifetime in III-V Semiconductors Due To Saturation of Recombination Centers," *J. Appl. Phys.*, vol. 70 (1), p. 225, 1 July 1991.
23. K. L. Tan, M. S. Lundstrom, and M. R. Melloch, "Effect of impurity trapping on the capacitance-voltage characteristics of n-GaAs/N-AlGaAs heterojunctions," *Appl. Phys. Lett.*, vol. 48 (6), p. 428, Feb. 1986. See also the references therein.
24. H. C. Casey, Jr. and Frank Stern, "Concentration-Dependent Absorption and Spontaneous Emission of Heavily Doped GaAs," *J. Appl. Phys.*, vol. 47 (2), p. 631, February 1976.

CHAPTER 2

ASSESSMENT OF LIFETIMES IN MBE-GROWN N-GaAs

(A more detailed description of the behavior and analysis of double heterostructures can be found in Chapter 1 of this report.) In order to determine the quality of Purdue's n-type GaAs grown by molecular beam epitaxy (MBE), we have grown two series of double heterostructures (DHs) doped with silicon to concentrations of 10^{17} cm^{-3} and 10^{18} cm^{-3}. Figure 2.1 shows the basic DH structure, and Table 2.1 shows the DH thicknesses and the decay constants found from observing photoluminescence (PL) decay at SERI. The decay constants of the thickest DHs were longer than the theoretical radiative lifetime using a value for the radiative B coefficient of $B = 2.0 \times 10^{-10}$ cm^3/s. We find that the MBE films and interfaces are of good quality, though not as good as the MOCVD films grown by Dr. Hugh MacMillan of the Varian Research Center. We find that our material quality is sufficient to continue studies in high efficiency GaAs solar cells.

Under easily achievable conditions which produce a flat carrier distribution in the DH, one can express the decay constant of a DH as [1],

$$\frac{1}{\tau_{DH}} = \frac{1}{\tau_{bulk}} + \frac{2S}{d}, \tag{1a}$$

where the bulk lifetime is defined as

$$\frac{1}{\tau_{bulk}} = \frac{1}{\phi_r \tau_r} + \frac{1}{\tau_{SRH}} + \frac{1}{\tau_{Auger}}. \tag{1b}$$

Here, S is the average of the front and back interface recombination velocities, d is the DH thickness, and τ_{bulk} is made up of contributions from the radiative, SRH, and Auger mechanisms, respectively. Asbeck's recycling cofactor, ϕ_r, quantitatively accounts for the enhancement of the radiative lifetime due to photon recycling [2]. Equations (1) clearly show contributions to τ_{DH} from both the interfaces and from the several bulk mechanisms. The lifetime plotted in Figs. 2.2-2.4 are found by a least squares fit to 50 data points. The decays of the MBE DHs differ in that the decay constant continuously decreased as shown in Fig. 2.3, for example. The PL decays of the MBE DHs doped 10^{17} cm^{-3} were not measured at sufficiently low intensity to prevent saturation of SRH recombination centers such that an exponential decay would be obtained. It was impossible, therefore, to determine the device lifetimes from the lower intensity PL decay observed; thus, a *range* of τ_{DH} is entered in Table 2.1 in such cases.

Double Heterostructure Thicknesses and Decay Constants $N_D = 10^{17}$ cm^{-3} $\tau_r = 1/BN_D = 50$ ns		
DH Thickness(μm)	Low Intensity τ_{DH}	High Intensity τ_{DH}
0.5	10-23 ns	28 ± 3 ns
1.0	8-18 ns	30 ± 5 ns
4.0	25-50 ns	83 ± 3 ns

Table 2.1. List of targeted thicknesses, doping concentrations, and observed decay constants for the double heterostructures doped 10^{17} cm^{-3} for this study.

The observed PL decays of the MBE DHs behaved differently from those of the MOCVD films indicating differences in the dominant recombination mechanisms. We found MOCVD films doped $N_D \leq 10^{18}$ cm^{-3} to be dominated by radiative recombination. For the MBE DHs we find that the films doped to 10^{17} cm^{-3} showed evidence of Shockley-Read-Hall (SRH) recombination centers, as indicated by a non-exponential decay under high intensity illumination. The non-exponential decay is attributed to the saturation of SRH deep levels under high intensity, but not high injection conditions [3]. Under these conditions and if $\tau_n \gg \tau_p$, the deep levels can become emptied and the SRH recombination equation reduces to

$$R = \frac{\Delta p}{\frac{\Delta p}{N_D}\tau_n + \tau_p} \qquad (2)$$

where Δp is the excess carrier concentration, and the other symbols have their usual meanings. This shows that the effective SRH lifetime can be longer under high intensity illumination than τ_{SRH} under low intensity illumination. This saturation of SRH recombination centers was also observed in the thicker and more heavily doped DHs grown by MOCVD. An example of non-exponential PL decay for the MOCVD DHs is shown in Fig. 2.2 where two separable regions of differing decay constant are observed.

n-$Al_{0.3}Ga_{0.7}As$ $1x10^{18}$ cm^{-3} 600 Å

n-GaAs active layer

SL BSF $1x10^{18}$ cm^{-3}
20 periods
30 Å $Al_{0.33}Ga_{0.67}As$/20 Å GaAs

n-AlAs $1x10^{18}$ cm^{-3} 500 Å

p-GaAs $1x10^{17}$ cm^{-3} 1 μm

Semi-Insulating GaAs substrate

Figure 2.1. Basic structure of the double heterostructures grown by molecular beam epitaxy.

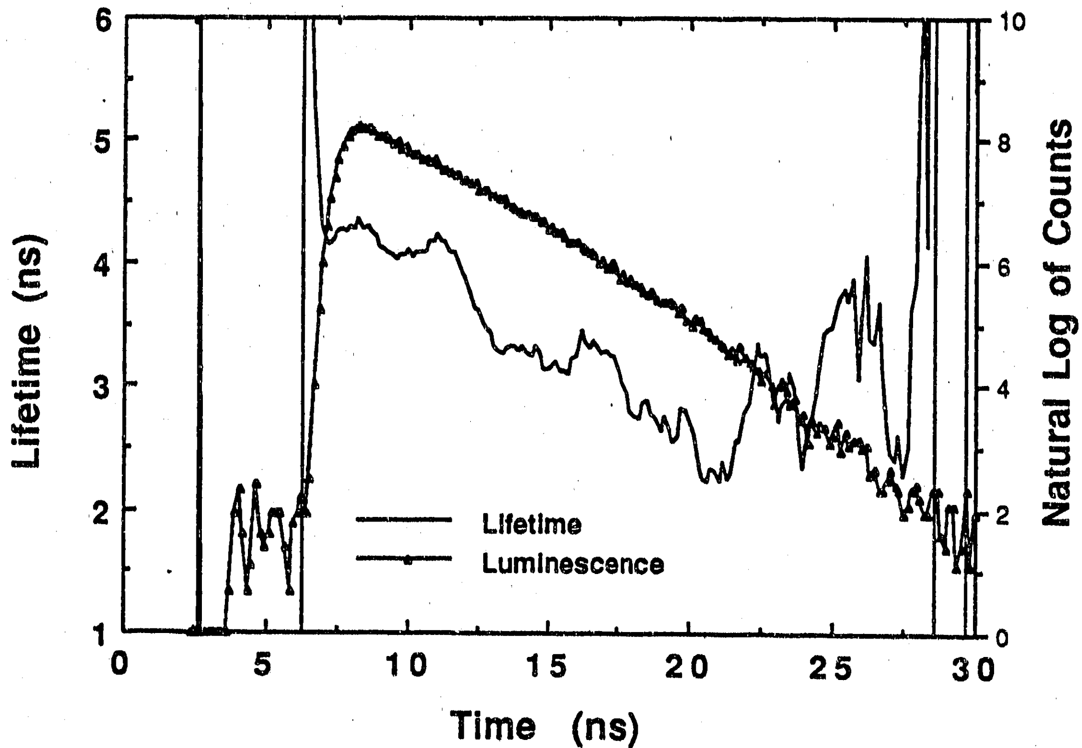

Figure 2.2. Photoluminescence decay for a 10 µm DH doped to 3.8×10^{18} cm^{-3}, grown by MOCVD, and under 10 milliwatts of excitation (high intensity). Note that there are two separable regions of differing decay constant, the initial one being approximately 4.1 nanoseconds, the second one being nearly 3.2 nanoseconds. Lifetimes versus time were computed by performing a least squares fit to 50 data points.

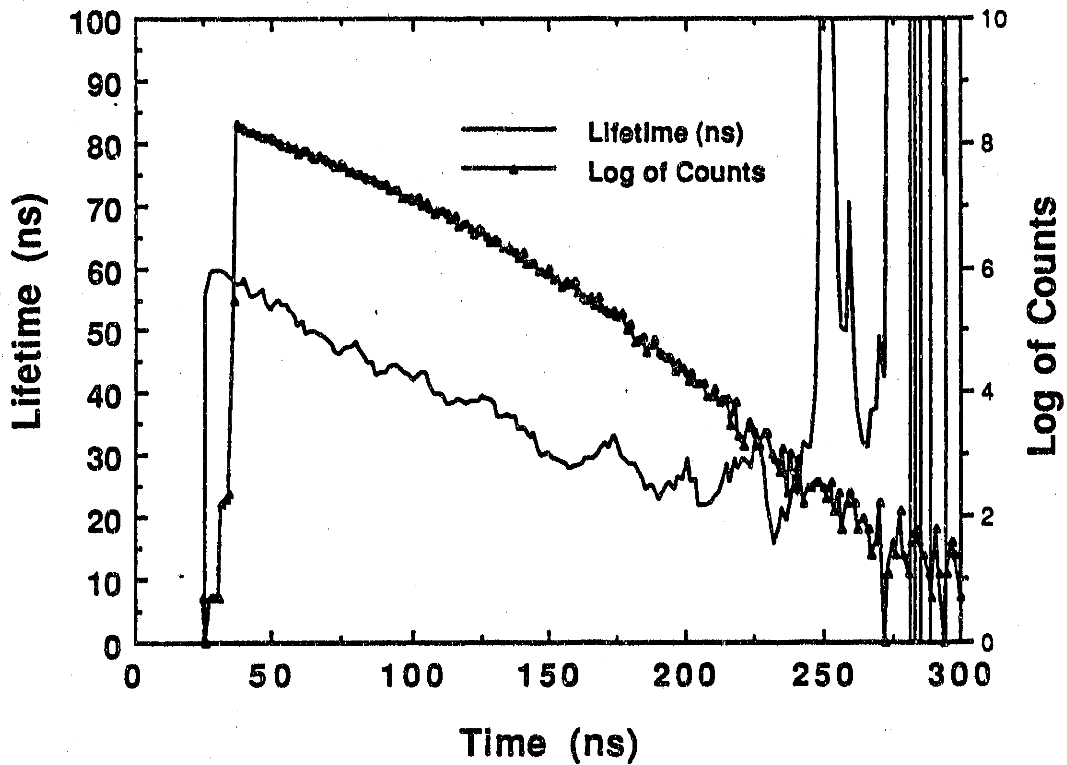

Figure 2.3. Photoluminescence decay for a 4 μm DH doped to 10^{17} cm^{-3} under 0.5 milliwatts of excitation (low intensity). The decay constant of this DH grown by MBE continuously decreases making a unique determination of τ_{DH} impossible. Lifetimes versus time were computed by performing a least squares fit to 50 data points.

Under high-intensity conditions, the PL decays showed an initial fast decay (typical of radiative recombination under high injection conditions) followed by an exponential decay. The plots of lifetime for these DHs are very noisy even if a large number of data points is used for the least-squares fit. Figure 2.4 is representative of these noisy data and the difficulty they present in determining τ_{DH}. A plot of $1/\tau_{DH}$ versus 2/d for the high intensity data is shown in Fig. 2.5; no corresponding plot for the low intensity data could be made because only a range of τ_{DH} could be deduced. The upper limit of the interface recombination velocity, S, deduced is 118 cm/s, which is small. (Interface recombination does not contribute significantly to the total recombination in the DHs.) Since there is so much uncertainty in the determination of τ_{DH} under high intensity for the DHs doped to 10^{17} cm^{-3}, this S should only be considered to be an order of magnitude result. The negative curvature displayed in Fig. 2.5 could be indicative of photon recycling; however, with only three data points available, it is difficult to say anything absolute.

The DHs doped to 10^{18} cm^{-3} showed exponential decays for most all intensities. Under high intensity, evidence of saturation of SRH recombination centers is observed, and we find that this is most prevalent for the thinnest DH. That the non-exponential decay is most prevalent in the thinnest DH grown by MBE indicates that the interfaces are the dominant recombination mechanism in these DHs. (For the MOCVD DHs, when we observed saturation of SRH centers, it was more prevalent for *thicker* samples. In this instance the effective radiative lifetime is enhanced by photon recycling, so the dominant recombination mechanism in the thicker DHs becomes SRH.)

Figure 2.6 shows $1/\tau_{DH}$ versus 2/d for the DHs doped 10^{18} cm^{-3}, under high and low intensities. Both of these plots are nearly linear, which is further evidence that the DHs are dominated by non-radiative recombination. (For DHs dominated by bulk recombination, such plots would show negative curvature (see Chapter 1) if radiative recombination and photon recycling were important.) Also, the S for the DHs under high intensity illumination is almost exactly half the value of S for the DHs under low intensity excitation, which further indicates that interface recombination centers are dominant and are becoming saturated. If the recombination centers saturate, the rate of recombination becomes dependent on both electron capture and hole capture, slowing the total process. Another noteworthy aspect seen in Fig. 2.6 is that the intercept for each of the linear fits is the same for both low and high intensity excitation. The inverse of the y-intercept would be the bulk lifetime if there is no photon recycling. (See Eqs. 1.) That τ_{bulk} does not change with intensity is an indication that the bulk material is dominated by radiative recombination. This "bulk lifetime" is approximately 12 nanoseconds which is comparable to that measured for the MOCVD films doped to $N_D = 10^{18}$ cm^{-3}. This is more than twice the lifetime that would be deduced from the often-used B-coefficient. (See Table 2.2.)

We find that the S of the DHs doped $N_D = 10^{18}$ cm^{-3} is significantly larger than that of the DHs doped $N_D = 10^{17}$ cm^{-3}. A similar but weaker trend was observed for the MOCVD DHs. That S would increase with increasing doping could be attributed to a reduction of the barrier at

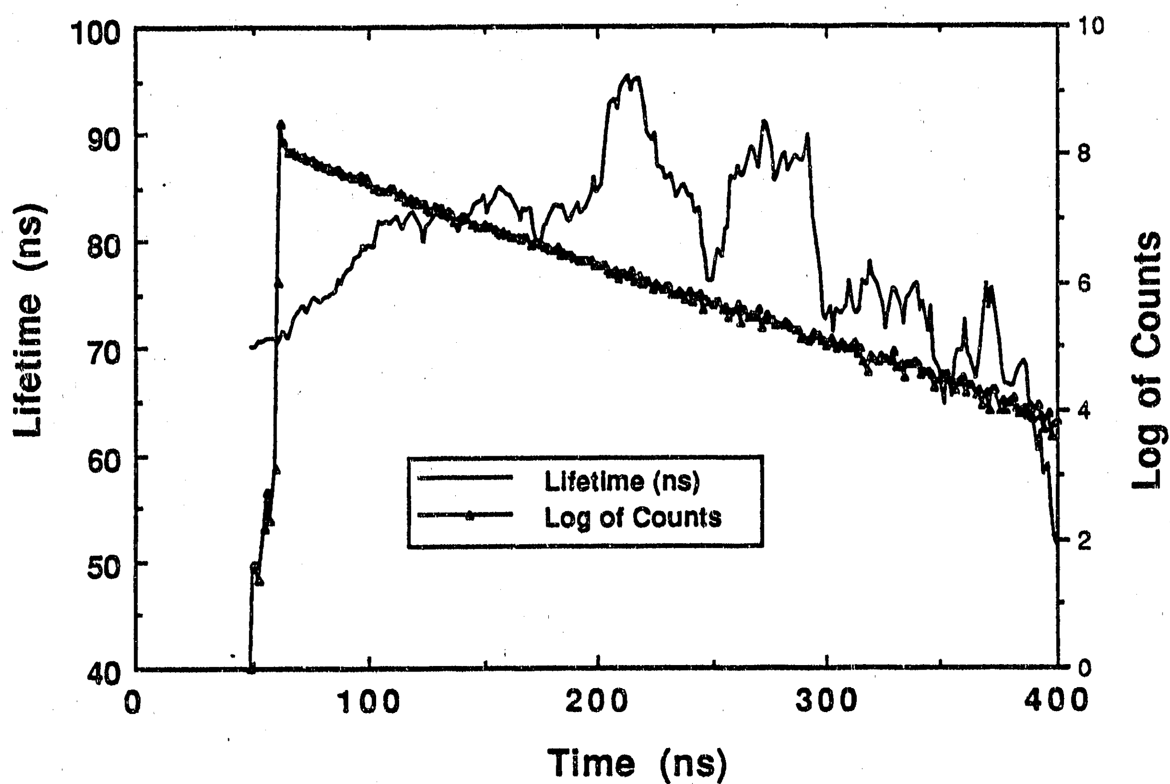

Figure 2.4. This is the same DH as was shown in Fig. 2.3, but the excitation power is 10 milliwatts here. The luminescence decay plots for these DHs are very noisy, even if a large number of data points is used for the least-squares fit. This figure is representative of the difficulty this noisy data presents in determining τ_{DH}. Lifetimes versus time were computed by performing a least squares fit to 50 data points.

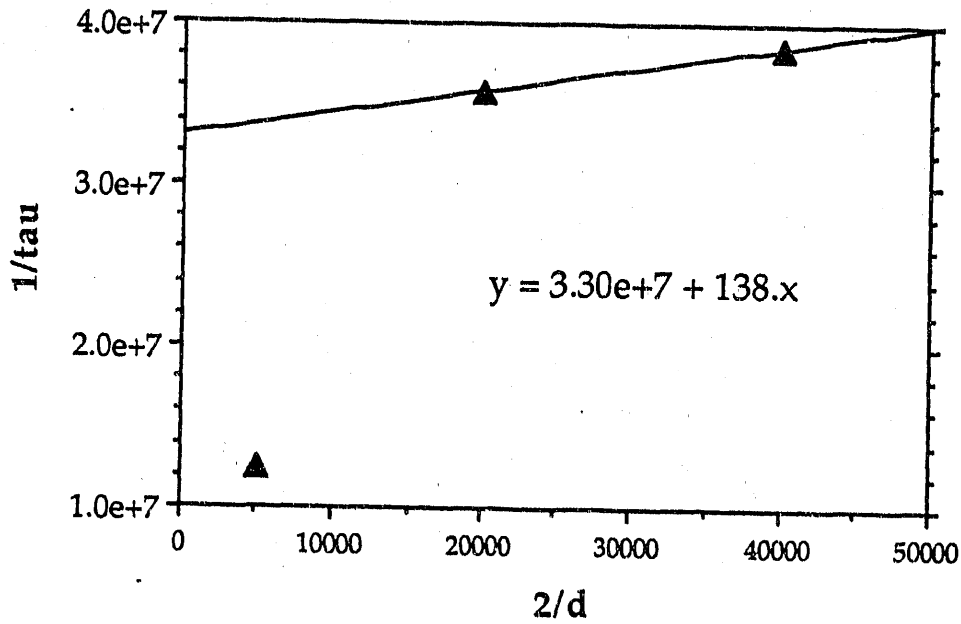

Figure 2.5. Plot of $1/\tau_{DH}$ versus 2/d for the high intensity data of the MBE DHs doped 10^{17} cm^{-3}. No corresponding plot for the low intensity data could be made because only a range of τ_{DH} was deduced. The upper limit of the interface recombination velocity, S, deduced is 138 cm/s, which is small.

Double Heterostructure Thicknesses and Decay Constants $N_D = 10^{18}$ cm^{-3} $\tau_r = 1/BN_D = 5$ ns			
DH Thickness(μm)	low intensity τ_{DH}	medium intensity τ_{DH}	high intensity τ_{DH}
0.25	2.5 ± 0.2 ns	2.7-3.8 ns	4.1 ± 0.3 ns
0.5	4.2 ± 0.5 ns	4.5-5.8 ns	5.8 ± 0.2 ns
2.0	7.8 ± 0.3 ns	---	9.5-10.7 ns

Table 2.2. List of targeted thicknesses, doping concentrations, and observed decay constants for the double heterostructures doped 10^{18} cm^{-3} for this study.

the GaAs/AlGaAs interfaces. The barrier for holes is smaller at higher doping concentrations because the equilibrium Fermi level of the n-GaAs is higher in the conduction band. The higher this GaAs Fermi level is in the conduction band, the smaller the potential barrier between the valence bands of the GaAs and AlGaAs layers become. This yields a barrier of smaller potential. While still able to confine minority holes in the GaAs active layer, a smaller potential barrier will allow more holes to reach the interface where recombination occurs.

In conclusion we have found that the lifetimes observed for our n-type GaAs grown by MBE are satisfactory for continuing our basic studies into high efficiency GaAs solar cells. At each doping concentration, we observed DH decay constants greater than those which would be deduced from the radiative limit using $B = 2.0 \times 10^{-10}$ cm^3/s. For DHs doped to $N_D = 10^{17}$ cm^{-3}, the interface contribution to the total recombination was small. Although S was significant for the DHs doped to $N_D = 10^{18}$ cm^{-3}, and this needs to be addressed, the bulk lifetime was as good as the best quality n-type GaAs.

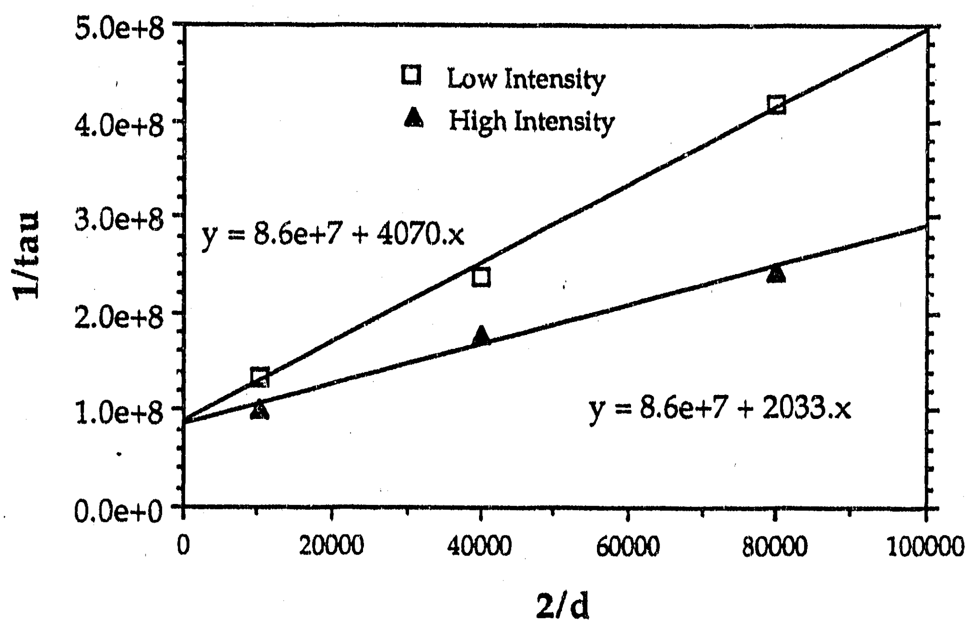

Figure 2.6. Plot of $1/\tau_{DH}$ versus 2/d for the DHs doped 10^{18} cm^{-3}, under both high and low intensities. Both of these plots are nearly linear which is evidence that the DHs are dominated by interface recombination. That τ_{bulk} (as found from the inverse of the y-intercept) does not change with intensity is an indication that the bulk material dominated by radiative recombination. The interface recombination velocities deduced are 4070 cm/s and 2033 cm/s for low and high intensities, respectively.

References

1. A. Many, Y. Goldstein, and N. B. Grover, *Semiconductor Surfaces*, John Wiley and Sons, New York, 1965.
2. P. Asbeck, "Self-absorption Effects on the Radiative Lifetime in GaAs-GaAlAs Double Heterostructures," *J. Appl. Phys.*, vol. 48 (2), p. 820, February 1977.
3. R. K. Ahrenkiel, B. M. Keyes, and D. J. Dunlavy, "Intensity-Dependent Minority-Carrier Lifetime in III-V Semiconductors Due To Saturation of Recombination Centers," *J. Appl. Phys.*, vol. 70 (1), p. 225, 1 July 1991.

CHAPTER 3

BASELINE AlGaAs CELL FABRICATION PROCESS

Summary

With the addition of an antireflection coating system, we are now fully capable of fabrication and analysis III-V solar cells here at Purdue. This chapter of the report discusses the basic processing steps used to fabricate the x=0.2 and x=0.4 Al mole fraction AlGaAs solar cells, highlighting the changes we have made to our standard GaAs diode processing. Significant changes were made to the metallization technique in order to ensure low-resistance contacts. Changes were made to the photolithography steps for compatibility with AlGaAs. Although we are not able as yet to test solar cell efficiency, we can project the efficiency of solar cells from the measured dark I-V and internal quantum efficiency. The results of such projections provide insight into the loss mechanisms of the cell, and serve to guide subsequent fabrication efforts.

3.1 Film Growth and Processing

Our Varian Gen II system for molecular beam epitaxy (MBE) has produced record quality $Al_{0.22}Ga_{0.78}As$ solar cells [1]. It has been shown that high growth temperatures yield higher quality AlGaAs [2] and we are still exploring that avenue. Design improvements could include a semiconductor stack reflector (SSR) [3], which would double as a back surface field, improving collection efficiency and thus cell efficiency. The emphasis in process development has been to avoid inadvertent degradation of the material quality, and subsequent device performance, by careful selection of process steps, techniques, and sequences.

A detailed process run sheet for our solar cell fabrication is in Appendix 1. An overview of the major processing steps in the fabrication of a solar cell is as follows:

1. Substrate mounting onto a Si wafer with indium.
2. Resist application and patterning for metal lift-off.
3. Pre-evaporation surface treatment in NH_4OH : DI.
4. Metal evaporation and resist lift-off.
5. Device evaluation: contact resistivity, metal thickness.
6. Resist application and patterning for mesa definition.
7. Mesa etch, using $H_2O_2 : H_2O : H_2SO_4 : CH_3OH$. Resist removal.
8. Device evaluation: mesa height, dark IV.
9. Cap Etch, using Citric acid and H_2O_2.
10. Optional antireflection coating with MgF_2 and ZnS, followed by a resist step to open contact window.

11. Quantum efficiency and dark I-V measurements, efficiency analysis.

3.1.1 Metal Definition

The first processing step is to prepare the sample for metallization. We expose using a darkfield mask to define the metal pattern for the solar cells and test devices such as varying area diodes and transmission lines. The chlorobenzene soak treats the photoresist so that excess metal can be subsequently lifted off. AZ 351 developer is found to be best suited for AlGaAs work. For GaAs processing American Hoescht AZ developer can be used, but AZ developer etches AlGaAs.

The next step removes the native oxide. Originally, we used a 1:40 NH_4OH : DI solution; the sample was immersed for 1 minute immediately before loading into the metal evaporation system. However, contact resistance studies showed poor and inconsistent contacts when this treatment was used. We found that increasing the concentration to 1:5 NH_4OH : DI resulted in contacts with consistently lower resistance. The sample is soaked for one minute then immediately loaded into the metal evaporation system.

We perform metallization in a Varian 4-pocket electron-gun evaporation system. The system is cryopumped while under high vacuum, and roughed using a combination of dry-vane mechanical and LN_2 sorption pumps. Source to sample distance is approximately 11 inches. System cycle time from roughing to unloading is typically eight hours. The electron gun is powered by a 6 KW, 6 KV dc supply, and the gun itself is an older 270° style.

The desired metal is evaporated, and the excess is lifted off by immersion in acetone. Our desired contact metal is Au which is evaporated onto a thin barrier metal. We have been using Ti as the barrier metal to prevent diffusion of the Au into the AlGaAs where it would form mid-gap recombination centers.

Ideally, the contacts need to be low in contact resistance, and also low in finger resistance. By evaporating 100 Angstroms (Å) of Ti and 1000 Å of Au, we obtain contact resistances as low as 3.0×10^{-3} ohm-cm^2. We realized that our finger resistance would be too high and calculate that using 10,000 Å of gold will yield finger resistances low enough to contribute no more than approximately a 0.3% loss in overall cell efficiency. However, we believe that 10,000 Å of Au will be too thick to lift off. 5000 Å will yield an efficiency loss of no more than 0.6%. By increasing resist exposure time, and with the help of the chlorobenzene soak, the 5000 Å of gold lifts off without difficulty.

Originally, we used a 30 second anneal at 400°C to improve contact resistance. This anneal usually decreased the contact resistance by an order of magnitude. We found, however, that the improvement in contact resistivity was less pronounced in the case of annealing the thicker (5000 Å) metal. One solution was to increase the anneal temperature. But the 100 Å of Ti might no longer act as a barrier, and so there might be spiking (and diffusion) of the Au into the material. When annealing above 400°C, we observed an increase in contact resistance, and in shunt current leakage. Presently, we are experimenting with thicker Ti layers in order to allow an increase in the anneal temperature. In addition, we will attempt to increase the

thickness of the Au too, subject to the limitation of the resist lift-off step. All of these measures will further reduce series resistance.

At this point we do some contact resistance measurements to see if the contacts are linear and low in resistance. The measurements are made using the same test setup as described below under "Dark I-V Measurements". Our cell masks include a variable-gap, transmission-line structure [4], which provides a convenient means for characterizing contact resistivity, as well as for checking contact linearity.

3.1.2 Mesa Definition

The current of the solar cell as well as the test devices, must be confined to the area of the device. A light field mask is used to define the so-called mesa patterns. Once again the run sheet supplies the steps used in this fabrication step. The etch rate has been found to be temperature dependent (quite possibly an Arrhenius relationship, although this has not been quantified), and is material dependent. If the solution is used within an hour of mixing, this etch rate is reasonably predictable (otherwise the solution becomes weak, possibly due to peroxide breakdown). Using a conservative estimate for the etch rate, a short etch is performed. Etch rates are computed after determining the mesa height using a Tencor Alpha-Step profilometer. The wafers are etched down to the middle of the base or beyond. This provides isolation from the other devices.

3.1.3 Cap Etch

The highly-doped, GaAs contacting layer or cap layer of the solar cell material is added at the end of film growth to protect the thin window layer of $Al_{0.8}Ga_{0.2}As$ from reaction and oxidation with the surrounding air, and to ensure better ohmic contacts. The cap material is GaAs, about 500-1000 Angstroms thick. The GaAs cap is removed using a highly selective citric acid/hydrogen peroxide etch [5,6]. At high citric acid/H_2O_2 ratios (i.e. 5-10:1) GaAs will etch 2-3 orders of magnitude faster than certain mole fractions of AlGaAs. Although it has not been quantified, observation has shown no noticeable removal of the $Al_{0.8}Ga_{0.2}As$ window layer.

Removal of the cap layer begins with determining the desired etch rate. The ratio of chemicals is chosen so that the etch rate is fast, but that the selectivity is high so that previously exposed AlGaAs around the mesa etches very little. The optical properties of GaAs and AlGaAs aid in determining the end of the etch. The GaAs undergoes color changes throughout the etch (mostly shades of purple). It is often easy to see the termination of the etch. The exposed $Al_{0.8}Ga_{0.2}As$ surface is darker than bare GaAs, flagging the total removal of the GaAs.

Further observations were made and noted about the citric acid/H_2O_2 etch. When the initial DI/citric acid solution is mixed, the reaction is endothermic. The DI/citric acid mixture is 1 ml : 1 g. Therefore, much heat is required to dissolve the citric acid reagent. The solution will appear to saturate, but patient magnetic stirring will dissolve all of the reagent. After this solution is mixed, the chosen volume of H_2O_2 is added. More stirring should follow. In addition, the etchant should be warmed to room temperature or a bit above. The heating of the etchant

increases the etch rate, but the rate can still be properly monitored and controlled. The etch is somewhat non-uniform. It is not clear if this is due to growth defects or innate inhomogeneities in the etchant. But the etch becomes somewhat more uniform when the solution is heated. The window layer is still not noticeably etched when the etchant is heated.

3.1.4 Antireflection Coating

The final step in processing of the solar cell is the addition of the anti-reflection (AR) coating. The main purpose of the coating is to suppress reflection of the incident sunlight. The coating also protects the window layer, which oxidizes quickly with exposure to air.

Our AR coatings are evaporated using a Varian "S-gun" sputter-coating system which has been converted into a thermal evaporator. The source materials are MgF_2 and ZnS, and are loaded into a Mo boat and a Ta "SiO furnace", respectively. The SiO furnace is used for the ZnS because of difficulty in obtaining acceptable evaporation performance using a conventional boat [7]. The sources are located on and electrically fed through the former S-gun target platform, near the bottom center of the chamber.

An aluminum sample holder was fabricated to replace the 3" wafer planets that came with the system. The holder was designed to incorporate the Inficon crystal thickness monitor head, which is also used to maintain the sample holder below ambient temperature by way of the crystal monitor's cooling water lines. This is believed to be important in maintaining a consistent and usable sticking coefficient for the ZnS evaporation [7,8]. The holder is large enough to hold several samples which face the sources directly and are the same distance from the sources as is the monitor crystal. Tungsten clips retain the samples in this upside-down configuration, near the center of the chamber.

The system is diffusion-pumped, with a large mechanical backing and roughing pump. A LN_2 cryotrap is located between the diffusion pump and the chamber, as well. Base pressure of the system with sources loaded and cool is approximately 1.0×10^{-7} Torr in the chamber, and 3.0×10^{-8} Torr below the gate valve.

The two-layer AR coating was chosen after Yoshikawa and Kasai [9]. Target film thicknesses are 570 Å for the ZnS layer, and 1000 Å for the MgF_2. Test evaporations have demonstrated excellent agreement between the thicknesses of deposited films (measured by profilometry) and those indicated by the Inficon XMS-1 film thickness monitor.

3.2 Characterization

3.2.1 Dark I-V Measurement

Electro-optical characterizations occur both during and after processing. Once the mesa-definition etch has been successfully performed, a dark I-V measurement can be made. We perform this measurement using a Micromanipulator probing station and an HP 4145B Semiconductor Parameter Analyzer. An example of the resulting data from such a measurement is shown in Fig. 3.1.

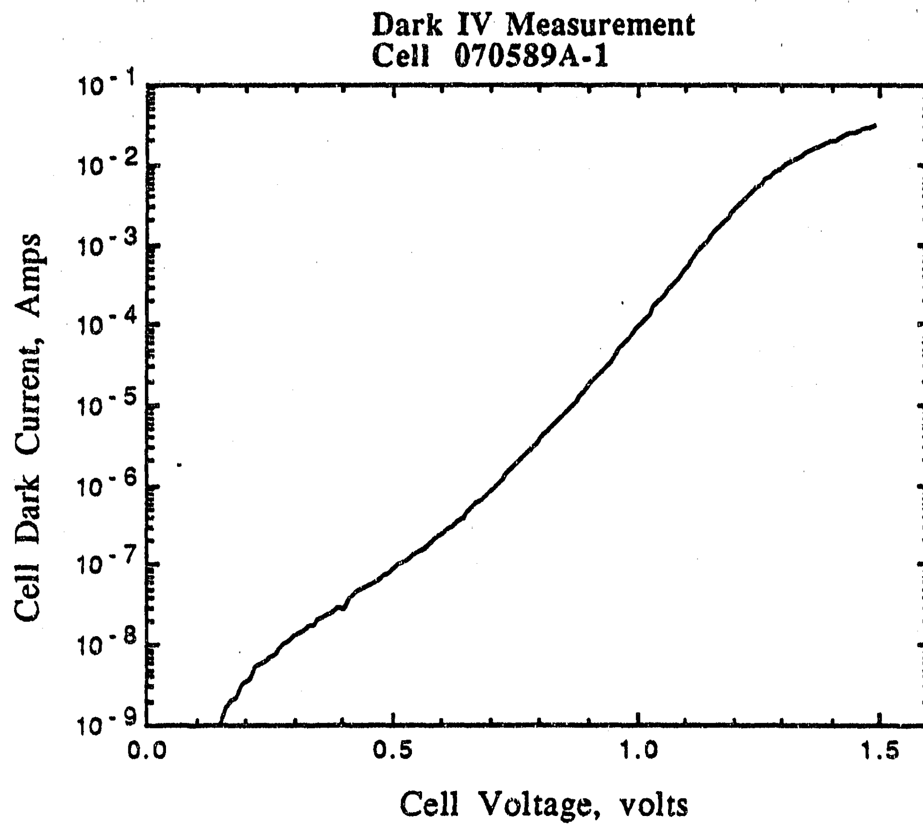

Figure 3.1. Dark IV Measurement for $Al_{0.22}Ga_{0.78}As$ solar cell.

These data are necessary for evaluating the performance of the solar cell and for characterization of the material and the junction. In addition, this same measurement setup is useful in determining the quality and resistance of our ohmic contacts, and the degree of isolation afforded by the mesa etch.

Difficulties with inconsistent probing resistances required a change to a four-probe I-V technique. At first, our measurements were made using two probes, one contacting the probe pad on the device front, and the other contacting the indium upon which the substrate is mounted. Using four probes proved a satisfactory solution for eliminating probe resistance from the measurements.

The I-V data points are taken approximately every 10 mV, and the upper voltage limit is chosen such that the estimated one-sun cell short-circuit current, Isc is exceeded. The dark I-V data are necessary for projecting cell efficiency after quantum efficiency measurements are made.

Separate perimeter over area (P/A) analyses can also be performed to separate perimeter and bulk components of the dark current [10]. We have not yet been concerned with these measurements, but expect them to be important in loss analysis. We will use them for further cell characterization as well as determinants for mesa heights and perimeter exposure.

3.2.2 Quantum Efficiency Measurement

Internal quantum efficiency is a measure of the ability of a solar cell to collect electron-hole pairs generated by monochromatic light. The results, presented as a function of wavelength, are crucial to projecting cell efficiency and also allow extraction of material and interface parameters. A block diagram of our optical setup for measuring internal quantum efficiency is shown in Fig. 3.2.

Legend for Fig. 3.2:

A:	1000 Watt Halogen Lamp with enclosure
S,F,L,I:	Oriel 77260 lens-filter-shutter assy., with adjustable iris
F1:	Front surface curved mirror, Rc = 1.0 m
F2:	Front surface curved mirror, Rc = 0.6 m
D:	Newport Research 818-SL silicon photodetector
DS:	Oriel 7070 Detection system
SL:	input and output monochromator slits, 0.3 cm
M:	Orien 77250 Monochromator, with 1200 lines/mm grating and 78200 Drive unit

After the cap has been successfully etched from the cell, a quantum efficiency measurement is initiated promptly, to avoid possible window degradation from atmospheric oxidation. The sample is illuminated by wavelengths ranging from 400 nm to 1000 nm in 10 nm steps, and

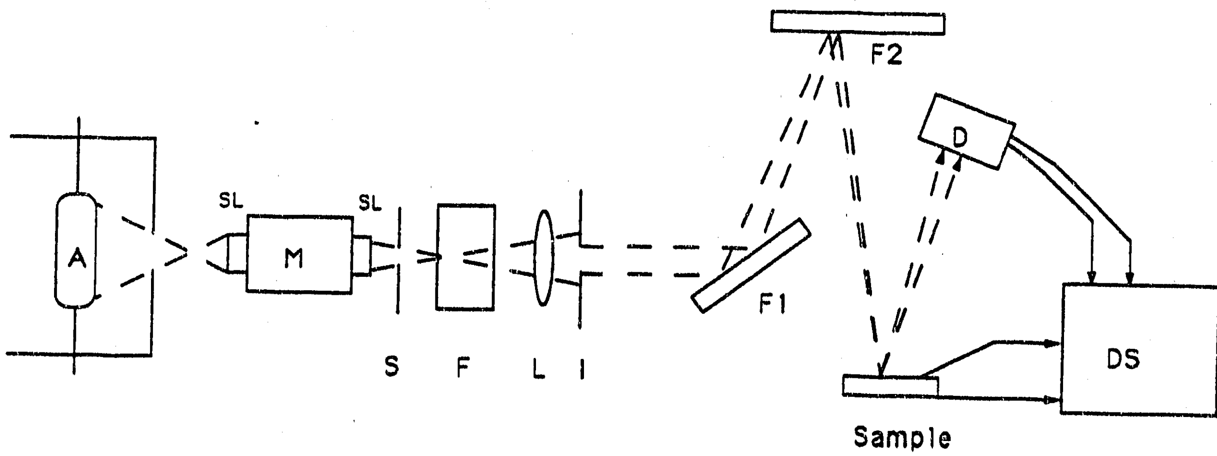

Figure 3.2. Quantum Efficiency Measurement System

the cell current is recorded from the detection system readout. Device reflectivity is similarly recorded for the same wavelengths. Finally, the sample is replaced in the setup by the detector, and the wavelengths are again scanned to obtain the incident photon intensity. These three sets of readings are then input to a program designed to plot the cell's external and internal quantum efficiency and reflectance vs. wavelength.

The QE measurement is used during processing to check the quality of the material. One mesa-isolated device is chosen and the GaAs cap layer removed. Thereafter, if the cell performance, as indicated by a good IQE plot, appears promising, the cap layer on the remainder of the sample is etched away, and an AR coating is promptly deposited.

A representative quantum efficiency plot is shown in Fig. 3.3, for a cell that was fabricated on a $Al_{0.2}Ga_{0.8}As$ MBE-grown film. This cell did undergo the cap etch, but no AR coating was applied.

3.2.3 Efficiency Projection and Computer Simulation

Although we cannot measure the efficiency of a solar cell directly, electro-optic characterization yields information about the film quality (diffusion lengths and interface recombination velocities), and allows us to project the expected efficiency of the processed solar cell. The measured IQE can be used to extract the emitter and base diffusion lengths (L_e and L_b, respectively) and interface recombination velocities (S_e and S_b, respectively). This information is vital to critically analyze the design of a solar cell toward improving its efficiency. Diffusion lengths and interface recombination velocities are found by performing a theoretical fit to the IQE using the equations of Hovel and Woodall [11] modified for a finite base length. Fig. 3.4 is an example of IQE data for a GaAs solar cell [12] and the theoretical fit to that data which yields the diode parameters listed. Values of S_e and L_e are not unique (nor are S_b and L_b), but upper limits on S and lower limits on L are found.

The measured IQE can also be integrated over the appropriate solar spectrum to compute the expected short-circuit current, J_{sc}. From this, the maximum power point is determined by superposing J_{sc} with the measured dark IV by finding the voltage at which the I-V product in Eq. 1 reaches its maximum.

$$P = V_{applied} \times (AJ_{sc} - I_{dark}) \tag{1}$$

Here, P is the power delivered by the solar cell, A is the area of the cell, $V_{applied}$ is the applied voltage and I_{dark} is the dark current. In order for superposition to work, we must either know the series resistance or we must only apply superposition in regions where series resistance negligibly affects the dark IV data. One can only find the V_{oc} or the fill factor (FF) by superposition if one knows the value of the series resistance.

As an example of how we project cell efficiency, we analyze our record efficiency $Al_{0.22}Ga_{0.78}As$ solar cell [1]. Table 1 lists the cell parameters as determined by experiment and by our simulations. The excellent agreement shows that our models sufficiently describe the solar cell performance to be accurate measures of expected efficiency.

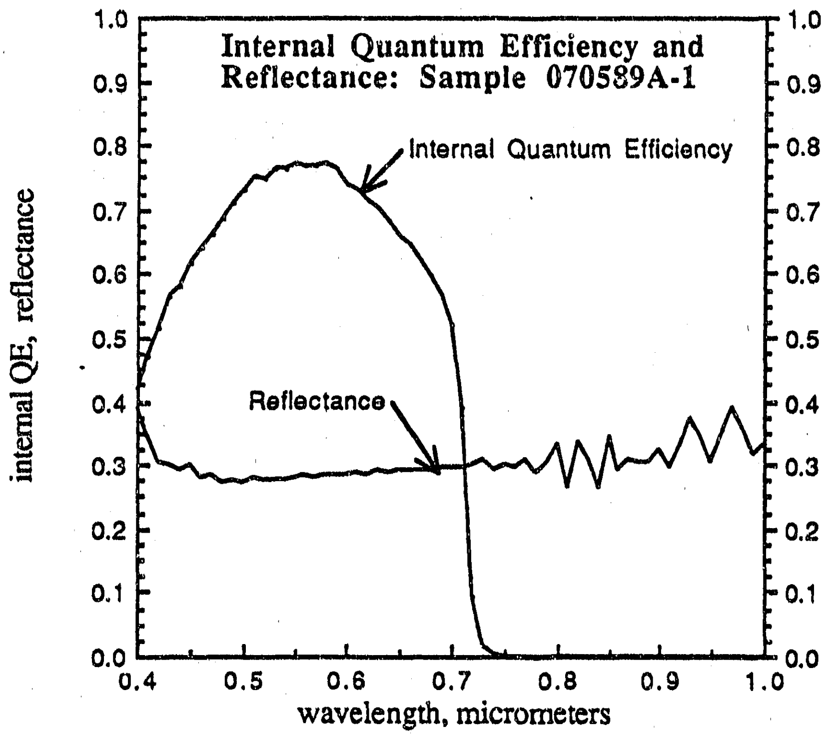

Figure 3.3. Quantum efficiency measurement plot for $Al_{0.22}Ga_{0.78}As$ solar cell

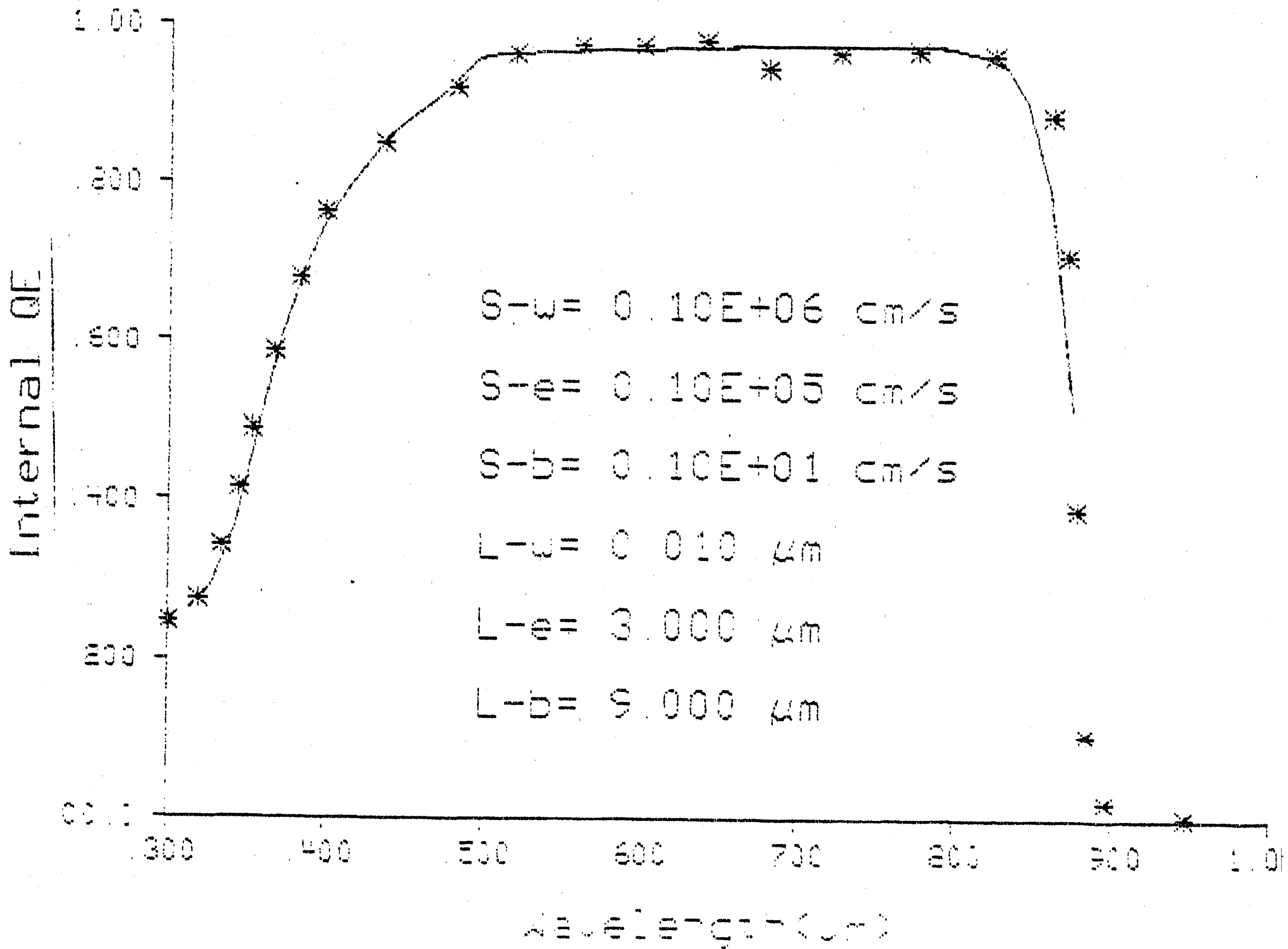

Figure 3.4. Sample IQE data for a GaAs solar cell [12] and the theoretical fit to that data which yields the solar cell parameters.

$Al_{0.22}Ga_{0.78}As$ Solar Cell Parameters		
---	Measured	Projected
V_{oc}	1.22 Volts	1.21 Volts
J_{sc}	16.3 mA/cm^2	16.1 mA/cm^2
FF	81%	80%
Eff	16.1%	15.6%

Table 1.1 Comparison of measured solar cell parameters and those projected using internal quantum efficiency and dark IV data.

References

[1] M. R. Melloch, S. P. Tobin, C. Bajgar, A. Keshavarsi, T. B. Stellwag, G. B. Lush, M. S. Lundstrom, and K. Emery, "High Efficiency $Al_{0.22}Ga_{0.78}As$ Solar Cells Grown by Molecular Beam Epitaxy," *Appl. Phys. Lett.*, July 1990.

[2] Amano, Ando, and Yamaguchi, "The effect of oxygen on the properties of AlGaAs solar cells grown by MBE," *J. Appl. Phys.*, **63** (8), April 1988.

[3] D. Boetz, L. M. Zinkiewicz, T. J. Roth, L. J. Mawst, and G. Peterson, "Low-Threshold-Current-Density Vertical-Cavity Surface-Emitting AlGaAs/GaAs Diode Lasers," *IEEE Photonics Tech. Lett.*, vol. 1 (8), p. 205, August 1989.

[4] Mak, Rogers, and Northrop, "Specific contact resistance measurements on semiconductors," *J. Phys. E: Scientific Instrumentation*, **22** (1989), pp. 317-321.

[5] C. Juang, K. J. Kuhn, and R. B. Darling, "Selective etching of GaAs and $Al_{0.3}Ga_{0.7}As$ with citric acid/hydrogen peroxide solutions," *J. Vac. Sci. Technol. B*, vol. 8 (5), p. 1122, Sept./Oct. 1990.

[6] M. Tong, D. Ballegeer, A. Ketterson, E. J. Roan, I. Adesida, and K. Y. Cheng, *A Comparative Study of Wet and Dry Selective Etching Processes for GaAs/AlGaAs/InGaAs Pseudomorphic MODFETs*, June 1991. Presented at the Electronic Materials Conference.

[7] S. Kurtz, Solar Energy Research Institute, private communication.

[8] S. Tobin, Spire Corp., private communication.

[9] Yoshikawa and Kasai, "Optimum design for window layer thickness of GaAlAs-GaAs heteroface solar cell regarding the effect of reflection loss," *J. Appl. Phys.* **52** (6), June 1981, pp. 4345-4347.

[10] P. Dodd, T. Stellwag, M. R. Melloch and M. S. Lundstrom, "Surface and perimeter recombination in GaAs diodes: an experimental and theoretical investigation," *IEEE Trans. Electron Devices*, ED-38 (6), June 1991.

[11] H. J. Hovel and J. M. Woodall, "Theoretical and Experimental Evaluations of $Ga_{1-x}Al_xAs$-GaAs Solar Cells," *Conf. Rec., 10th IEEE Photovoltaic Specialists Conf.*, p. 25, IEEE, New York, 1973.

[12] S. P. Tobin, S. N. Vernon, C. Bajgar, S. J. Wojtczuk, M. R. Melloch, A. Keshavarzi, T. B. Stellwag, S. Venkatesan, M. S. Lundstrom, and K. E. Emery, "Assessment of MOCVD- and MBE-Grown GaAs for High-Efficiency Solar Cell Applications," *IEEE Trans. Elec. Devices*, vol. 37, p. 469, 1990.

Appendix 1
AlGaAs Solar Cell Run Sheet
June 1991

A. Mounting Steps

- Wear a respirator mask in addition to normal protective wear (whenever cleaving any GaAs)
- Cleave the necessary sample size using a razor blade.
- Heat a Si wafer and In pellets on a hot plate until In melts. The setting is about half-way on most hot plates. Do not use a high heat setting for the In will oxidize.
- Use a razor blade to spread the In.
- Place the sample onto the In. Move the sample around to insure that the In is in contact with the back of the sample.
- Remove the mounted sample and allow to cool.

B. Metal Mask steps

- Wafer clean
  a. 5 minutes ACE
  b. 5 minutes TCA
  c. 5 minutes METH
  d. DI rinse and blow dry with N_2
  (Remember, never let anything dry on GaAs. Always blow dry!)
- Hardbake at 120°C for 15 minutes.
- Spin wafer at 3500 RPM for 40 seconds and blow with N_2 to remove stray dust particles.
- Spin on AZ1350J-SF photoresist at 3500 RPM for 40 seconds. (The resist thickness is about 2 microns). Using of a 1 micron filter is recommended.
- Softbake at 85°C for 15 minutes (the temperature and time are critical for the lift-off process.)
- Expose dark field metal mask. For desired thicknesses of up to 5000 Angstroms use 7.5 seconds of the Suss mask aligner. For thicknesses of 5000-10000 Angstroms use 10 seconds. (Constant intensity setting, 23.0 mw/cm^2.)
- Soak in chlorobenzene. For up to 5000 Angstrom metal thicknesses, soak for 15 minutes. For up to 10000 Angstroms use a 17 minute soak. Blow dry with N_2, but do not use a DI rinse.
- Develop photoresist in AZ351 developer and DI (1:5) until contacts clear. Use a microscope to determine when the contacts are clear. It generally takes 30 to 60 seconds. Use iterations.
- DO NOT do a hardbake.

C. Metal Evaporation and Lift-Off

- Remove native oxide in [1:5 NH_3OH:DI] for 1 minute. Rinse with DI and blow dry with N_2.
- Load into Varian e-beam and pump down to at most 3×10^{-6} Torr.
- Follow e-beam write-up to evaporate desired metal. Generally, 500 Angstroms of Ti is evaporated for a barrier layer. Au thicknesses are chosen to minimize resistance.

- Lift-off excess metal in ACE. Use a ACE filled squirt bottle to encourage process.
- Rinse in METH then DI. Blow dry with N_2.
- Inspect using a microscope to insure metal between cell fingers and test structures is removed. Use iterations to remove excess.
- Use a rapid thermal anneal to create better ohmic contacts. Use 400°C for 30 seconds.

D. Mesa Mask Steps

- Wafer clean
  a. 5 minutes ACE
  b. 5 minutes TCA
  c. 5 minutes METH
  d. DI rinse and blow dry with N_2
- Hardbake at 120°C for 15 minutes.
- Spin wafer at 3500 RPM for 40 seconds and blow with N_2 to remove stray dust particles.
- Spin on AZ1350-SF photoresist at 3500 RPM for 40 seconds. (The resist thickness is about 2 microns). Use of a 1 micron filter is recommended.
- Softbake at 85°C for 15 minutes.
- Align and expose light field meas mask. Use constant intensity exposure for 7.5 seconds on the Suss.
- Develop photoresist in AZ351 developer and DI (1:5) until contacts clear. Use a microscope to determine when the resist is clear. Make sure mesas completely cover the metal. It generally takes 30 to 60 seconds. Use iterations.
- Hardbake at 120°C for 15 minutes.
- Etch Mesas using DI, methanol, H_3PO_4, and H_2O_2 (1:1:1:1). Wait 20 minutes before Etching, to allow the solution to cool. Etch rate is about 2 microns/minute. Etch 30 seconds first.
- Use Tencor Alpha step to determine mesa height. (Assume a 2 micron resist thickness). The mesa needs to be etched to the junction into the base region or even beyond to ensure carrier isolation. Calculate etch rate.
- Etch again if necessary. Recalculate etch rate.
- Remove photoresist with a 5 minute ACE bath.
- Rinse in METH, then DI. Blow dry with N_2.

E. Dark I-V measurements

- Use the HP 4145 and micromanipulator probe station (or equivalent) to detemine dark I-V characteristics. Remember to use low resistance probes, or four probes, for solar cells!

F. Cap Etch

- Use AlGaAs/GaAs selective etchant to etch off cap layer. Mix 1 citric acid (by mass): 1 DI (by volume). Use magnetic stirrer to dissolve all citric acid. Warm solution to room temperature or above using a hot plate (the reaction is endothermic).
- Mix 8 Citric acid/DI : 1 H_2O_2 and stir.
- Etch rate is about 0.2 microns/min. Etch time depends on thickness of cap. The optical properties of GaAs/AlGaAs can be used to determine the etch's end. The surface will turn purple to green then almost black. The black surface means that the etch has

reached the window layer. Cease etching!

- Rinse in DI and blow dry with N_2.

G. Anti-Reflection Coating

- Load sample onto holder and mount holder onto the crystal monitor head.
- Close system; initiate pumpdown. Verify correct crystal monitor operation, and check density setting for ZnS.
- With system pressure in low 10^{-7} range, evaporate ZnS *slowly* until monitor reads 570 Angstroms.
- Reset crystal monitor, and reset density for MgF_2. Evaporate MgF_2 until it reads 1000 Å.
- Allow system to cool for 15 minutes, then bring to air and unload sample.

H. Quantum Efficiency Measurements

- Perform QE measurements on the Oriel system.
- Use dark IV data and QE data as input to efficiency analysis programs. Produce estimates of I_{sc}, V_{oc}, fill factor, and efficiency.

APPENDIX 2: BIBLIOGRAPHY OF SERI-SUPPORTED PUBLICATIONS

This appendix lists the various reports, theses, conference presentations, and journal publications that have resulted from research supported under this subcontract.

[1] G.B. Lush, H.F. MacMillan, B.M. Keyes, R.K. Ahrenkiel, M.R. Melloch, and M.S. Lundstrom, "Photoluminescence Decay Study of Minority Carrier Recombination in n-Type GaAs," presented at the 1991 Electronics Materials Conf., Boulder, Colorado, June, 1991.

[2] G.B. Lush, H.F. MacMillan, B.M. Keyes, R.K. Ahrenkiel, M.R. Melloch, and M.S. Lundstrom, "Measurement of Minority Carrier Lifetime in n-Type GaAs and the Implications for Solar Cells," to be presented at the 22nd IEEE Photovoltaic Spec. Conf., Las Vegas, Nevada, October, 1991.

[3] R.K. Ahrenkiel, B.M. Keyes, G.B. Lush, M.R. Melloch, M.S. Lundstrom, and H.F. MacMillan, "Hole Lifetime in GaAs," to be presented at the 1991 American Vacuum Society Annual Meeting, Seattle, Washington, November, 1991.

[4] G.B. Lush, H.F. MacMillan, B.M. Keyes, M.S. Lundstrom, R.K. Ahrenkiel, and M.R. Melloch, "A Study of Minority Carrier Lifetime versus Doping in N-Type GaAs Grown by Metalorganic Vapor Deposition," submitted for publication.

Document Control Page	1. NREL Report No. NREL/TP-451-4851	2. NTIS Accession No. DE92010558	3. Recipient's Accession No.

4. Title and Subtitle	5. Publication Date
New III-V Cell Design Approaches for Very High Efficiency	January 1993
	6.
7. Author(s) M.S. Lundstrom, M.R. Melloch, G.B. Lush, G.J. O'Bradovich, M.P. Young	8. Performing Organization Rept. No.
9. Performing Organization Name and Address Purdue University West Lafayette, Indiana 47907	10. Project/Task/Work Unit No. PV221103
	11. Contract (C) or Grant (G) No. (C) XM-0-19142-1 (G)
12. Sponsoring Organization Name and Address National Renewable Energy Laboratory 1617 Cole Blvd. Golden, CO 80401-3393	13. Type of Report & Period Covered Technical Report 1 August 1990 - 31 July 1991
	14.

15. Supplementary Notes
NREL technical monitor: J. Benner

16. Abstract (Limit: 200 words)

This report describes progress during the first year of a three-year project. The objective of the research is to examine new design approaches for achieving very high conversion efficiencies. The program is divided into two areas. The first centers on exploring new thin-film approaches specifically designed for III-V semiconductors. The second area centers on exploring design approaches for achieving high conversion efficiencies without requiring extremely high quality material. Research activities consisted of an experimental study of minority carrier recombination in n-type, metal-organic chemical vapor deposition (MOCVD)-deposited GaAs, an assessment of the minority carrier lifetimes in n-GaAs grown by molecular beam epitaxy, and developing a high-efficiency cell fabrication process.

17. Document Analysis
a. Descriptors
high efficiency ; photovoltaics ; solar cells ; semiconductors ; gallium arsenide

b. Identifiers/Open-Ended Terms

c. UC Categories
272

18. Availability Statement	19. No. of Pages
National Technical Information Service U.S. Department of Commerce 5285 Port Royal Road Springfield, VA 22161	54
	20. Price A04

Form No. 0069E (6-30-87)